Cell Stem Cell

Resource

Mapping Development of the Human Intestinal Niche at Single-Cell Resolution

Graphical Abstract

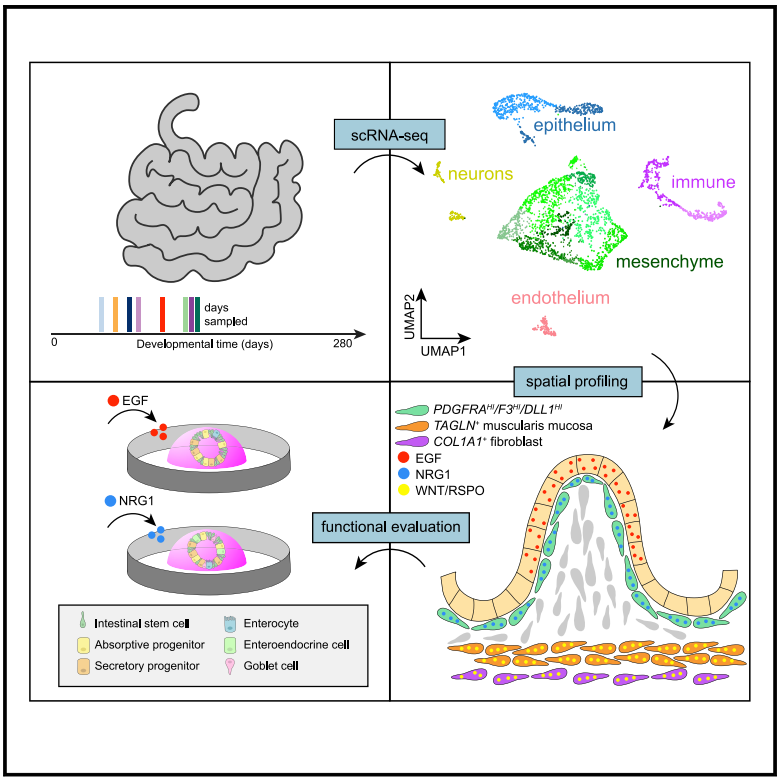

Authors

Emily M. Holloway, Michael Czerwinski, Yu-Hwai Tsai, ..., Barbara Treutlein, J. Gray Camp, Jason R. Spence

Correspondence

spencejr@umich.edu

In Brief

Holloway, Czerwinski, Tsai et al. used scRNA-seq to characterize the cellular diversity of the developing human intestinal stem cell niche. Transcriptional and spatial profiling demonstrated that *Neuregulin 1* (*NRG1*) is expressed by *PGDFRA*^{HI}/*F3*^{HI}/*DLL1*^{HI} subepithelial mesenchyme and that NRG1, but not EGF, permitted secretory lineage differentiation in enteroid culture.

Highlights

- Cell diversity in the developing human intestine was interrogated using scRNA-seq
- *PGDFRA*^{HI}/*F3*^{HI}/*DLL1*^{HI} mesenchyme lines the epithelium and expresses *NRG1*
- *EGF*, a common *in vitro* niche factor, is not abundant in the crypt domain
- Compared with EGF, NRG1 increases cellular diversity in enteroid culture

Holloway et al., 2021, Cell Stem Cell *28*, 568–580
March 4, 2021
https://doi.org/10.1016/j.stem.2020.11.008

CellPress

CellPress

Cell Stem Cell

Resource

Mapping Development of the Human Intestinal Niche at Single-Cell Resolution

Emily M. Holloway,[1,8] Michael Czerwinski,[2,8] Yu-Hwai Tsai,[2,8] Joshua H. Wu,[2] Angeline Wu,[2] Charlie J. Childs,[1] Katherine D. Walton,[1] Caden W. Sweet,[2] Qianhui Yu,[3] Ian Glass,[4] Barbara Treutlein,[5] J. Gray Camp,[3,6] and Jason R. Spence[1,2,7,9,*]

[1]Department of Cell and Developmental Biology, University of Michigan Medical School, Ann Arbor, MI 48109, USA
[2]Department of Internal Medicine, Gastroenterology, University of Michigan Medical School, Ann Arbor, MI 48109, USA
[3]Institute of Molecular and Clinical Ophthalmology Basel (IOB), Basel, Switzerland
[4]Department of Pediatrics, Genetic Medicine, University of Washington, Seattle, WA 98195, USA
[5]Department of Biosystems Science and Engineering, ETH Zürich, Basel, Switzerland
[6]University of Basel, Basel, Switzerland
[7]Department of Biomedical Engineering, University of Michigan College of Engineering, Ann Arbor, MI, USA
[8]These authors contributed equally
[9]Lead Contact
*Correspondence: spencejr@umich.edu
https://doi.org/10.1016/j.stem.2020.11.008

SUMMARY

The human intestinal stem cell niche supports self-renewal and epithelial function, but little is known about its development. We used single-cell mRNA sequencing with *in situ* validation approaches to interrogate human intestinal development from 7–21 weeks post conception, assigning molecular identities and spatial locations to cells and factors that comprise the niche. Smooth muscle cells of the *muscularis mucosa*, in close proximity to proliferative crypts, are a source of *WNT* and *RSPONDIN* ligands, whereas *EGF* is expressed far from crypts in the villus epithelium. Instead, an *PDGFRA*^{HI}/*F3*^{HI}/*DLL1*^{HI} mesenchymal population lines the crypt-villus axis and is the source of the epidermal growth factor (EGF) family member *NEUREGULIN1* (*NRG1*). In developing intestine enteroid cultures, NRG1, but not EGF, permitted increased cellular diversity via differentiation of secretory lineages. This work highlights the complexities of intestinal EGF/ERBB signaling and delineates key niche cells and signals of the developing intestine.

INTRODUCTION

The stem cell niche within a tissue is required to regulate stem cell maintenance, self-renewal, and differentiation (Scadden, 2006). The niche is made up of physical and chemical cues, including the extracellular matrix (ECM), cell-cell contacts, growth factors, and other small molecules, such as metabolites (Capeling et al., 2019; Cruz-Acuña et al., 2017; Gjorevski et al., 2016). Understanding the niche within various tissues has been central to understanding how tissues maintain homeostasis and how disease may occur (van de Wetering et al., 2002). Further, establishing proper *in vitro* niche conditions has allowed growth and expansion of gastrointestinal tissue-derived stem cells in culture (Dedhia et al., 2016; Kretzschmar and Clevers, 2016). For example, by understanding that WNT signaling is important for maintaining intestinal stem cell (ISC) homeostasis (Muncan et al., 2006; Pinto et al., 2003; Sansom et al., 2004), that blockade of Bone Morphogenetic Protein (BMP) signaling by NOGGIN (NOG) promotes ectopic crypt formation (Haramis et al., 2004), and that Epidermal Growth Factor (EGF) is a potent stimulator of proliferation (Goodlad et al., 1987; Ulshen et al., 1986), it was determined that WNTs, RSPONDINs (RSPOs), NOG, and EGF can be utilized to expand and maintain ISCs in culture as three-dimensional intestinal organoids (Ootani et al., 2009; Sato et al., 2009, 2011b). This information has been leveraged to expand and culture human pluripotent stem cell-derived intestinal organoids *in vitro* (Capeling et al., 2020; Finkbeiner et al., 2015; Spence et al., 2011; Wells and Spence, 2014).

Despite significant progress over the past decade, it is also clear that current *in vitro* systems are still not optimized to most accurately reflect the *in vivo* environment. Ongoing efforts are aimed at improving the *in vitro* physical environment by developing biomimetic ECM (Capeling et al., 2019; Cruz-Acuña et al., 2017; Gjorevski et al., 2016) and by adjusting signaling cues to more accurately reflect the *in vivo* niche (Fujii et al., 2018). More recently, single-cell technologies have started to reveal unprecedented amounts of information about the cellular heterogeneity of human intestinal tissue and the ISC niche during health and disease (Kinchen et al., 2018; Martin et al., 2019; Smillie et al., 2019) and will undoubtedly yield substantial information about cell types and niche cues that regulate ISCs in various contexts.

Here we set out to better understand the cellular diversity and niche cues of the developing human intestine by using single-cell

CellPress

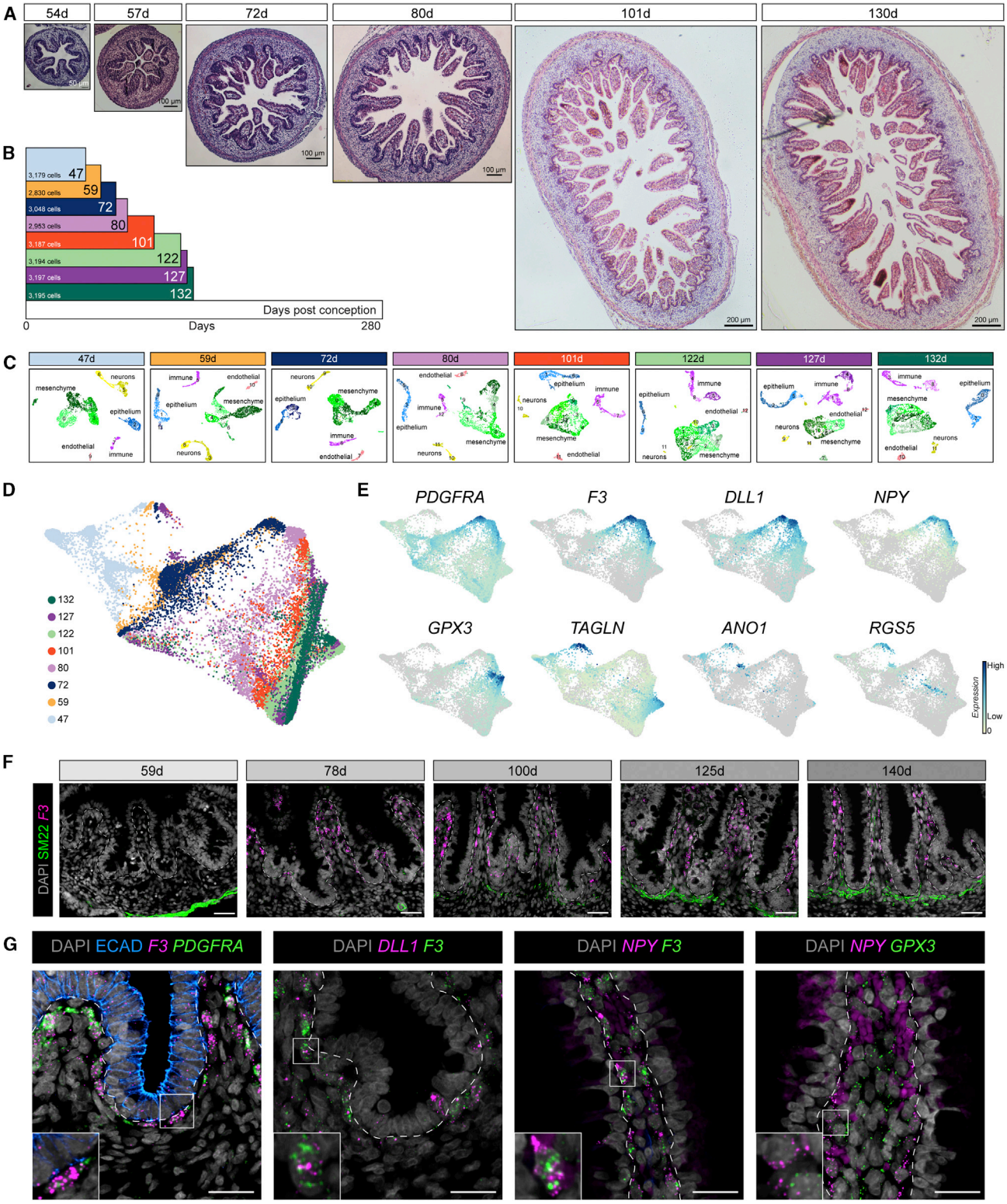

Figure 1. Mesenchymal Heterogeneity in the Developing Human Duodenum

(A) H&E staining on human fetal intestine sections at a constant scale spanning from 54–130 days post conception.

(B) Timeline of specimens and corresponding number of cells profiled by scRNA-seq after filtering and "cleaning" of ambient/background RNA (STAR Methods) (n = 8 biological specimens; n = 1 technical replicate 47, 59, 72, 80, 101, and 132 days; n = 2 technical replicates 122 and 127 days).

(legend continued on next page)

mRNA sequencing (scRNA-seq) to describe the cell-associated transcriptional signatures and by using fluorescence *in situ* hybridization (FISH) and immunofluorescence (IF) to define the location of cells and factors that make up the ISC niche. We sought to interrogate the cellular source of known stem cell niche factors and identify new niche factors. We determined that a source of WNT and RSPO ligands that reside just below the proliferative crypt domains is *ACTA2*$^{+}$/*TAGLN*$^{+}$ smooth muscle cells of the *muscularis mucosa*. We further determined that *EGF* is not expressed in the mesenchyme but is most abundant in the enterocytes of the villus epithelium, several cell diameters away from the proliferative region of the crypt. We identified a population of subepithelial cells (SECs) that lines the entire villus-crypt axis, marked by a *F3*^{HI}/*PDGFRA*^{HI}/*DLL1*^{HI} expression profile, and found that these cells express the EGF-family ligand *NEUREGULIN1* (*NRG1*), which has been implicated recently as an important regenerative cue in the murine intestine (Jardé et al., 2020). Given that *NRG1* is expressed in mesenchymal cells adjacent to proliferative crypts, we tested the effect of EGF and NRG1 on *in vitro* ISC growth using fetal human duodenal enteroids. We observed that EGF potently stimulated proliferation and primarily maintained enteroids as a stem/progenitor cell population, whereas NRG1 supported enteroid growth and enhanced cell type diversity. These results suggest that NRG1 acts as a niche cue that, when used in place of EGF, supports homeostasis *in vitro*, allowing stem cell maintenance and differentiation of human intestinal enteroids.

RESULTS

Interrogating the Developing Human Small Intestine at Single-Cell Resolution

Given that little is known about mesenchymal cell heterogeneity in the fetal human intestine, we aimed to better understand the mesenchymal cell populations that make up the developing human ISC niche. To do this, we obtained samples of human fetal duodenum or duodenum with adjacent proximal small intestine (in the case of very young tissues) starting just after onset of villus morphogenesis (47 days post conception) with samples interspersed up to the midpoint (132 days) of typical full-term (280 days) and performed histological and molecular analysis (Figures 1A and 1B). Major physical changes occur throughout this developmental window: rapid growth in length and girth along with formation of villi and crypt domains within the epithelium and increased organization and differentiation of smooth muscle layers within the mesenchyme (Chin et al., 2017; Figure 1A).

To capture the full complement of cell types that contribute to the developing human intestine, we dissociated full-thickness intestinal tissue from 8 specimens ranging between 47 and 132 days after conception and used scRNA-seq to sequence 2,830–3,197 cells per specimen after filtering and ambient RNA removal (STAR Methods). 24,783 total cells were used in the analysis after passing computational quality filtering (Figure 1B). Following dimensional reduction and visualization with uniform manifold approximation and projection (UMAP) (Becht et al., 2018; Wolf et al., 2018), we used canonical genes to annotate each sample individually by identifying major cell classes, including epithelial, mesenchymal, endothelial, enteric nervous, and immune cells (Figures 1C and S1A). To focus our analysis on the mesenchymal niche populations found in each sample, we computationally extracted and re-clustered the mesenchyme (1,462–2,054 cells per specimen) and annotated a population of *PDGFRA*^{HI} cells, which have also been described in mice (McCarthy et al., 2020), and *ACTA2*$^{+}$/*TAGLN*$^{+}$ smooth muscle cells (Figures 1E and S1C). We also identified additional sub-clusters and gene expression patterns not described previously in mice, which we describe in greater detail below (Figure S1C). Given the dramatic morphological changes that take place across this development time (Figure 1A), we implemented Harmony (Nowotschin et al., 2019), an algorithm that allows interrogation of scRNA-seq data across discrete time points (Figures 1D, 1E, and S1D).

Force-directed layouts following Harmony implementation ordered cells broadly according to their developmental age (days after conception) (Figure 1D). The day 47 cells were largely separate from other time points, with the exception of an *ACTA2*^{HI}/*TAGLN*^{HI}/*RGS5*$^{+}$ population of vascular smooth muscle cells (VSMCs) (Muhl et al., 2020; Figures 1D and 1E). Cells were then ordered according to developmental time, with cells from samples older than 101 days (101, 122, 127, and 132 days) clustering together. In addition to the VSMC population, this analysis suggested the emergence of several mesenchymal populations, including a *PDGFRA*^{HI}/*F3*^{HI}/*DLL1*^{HI} population, a *GPX3*^{HI} population, a *TAGLN*^{HI}/*RGS5*$^{-}$ smooth muscle population, and a prominent cluster of cells defined as fibroblasts based on their expression of *COLLAGEN* genes (*COL1A1* and *COL1A2)* and *DECORIN* (*DCN*) (Figures 1E and S1D; Kinchen et al., 2018). *F3* has been shown recently to be expressed in a population of mesenchymal cells that is adjacent to the human colonic epithelium (Kinchen et al., 2018), and these cells were additionally characterized by their enrichment of *NPY*, *DLL1*, *FRZB*, and *SOX6* (Figures 1E and S1B–S1D).

(C) UMAP visualization of each sample analyzed by scRNA-seq, displayed by age post conception. Cluster identities were assigned based on expression of canonical lineage markers (see also Figure S1). Mesenchymal (green), epithelial (blue), neuronal (yellow), immune (purple), and endothelial (pink) cell clusters were identified at all ages sequenced.

(D) Following application of Harmony to mesenchymal cells from all time points, a force-directed layout illustrates the relationship between time points. Cells are colored by sample identity (days post conception).

(E) Feature plots of individual genes for various lineages, including *PDGFRA*, *F3*, *DLL1*, *NPY*, *GPX3*, *TAGLN*, *ANO1*, and *RGS5*, plotted onto the force-directed layout presented in (D).

(F) Representative images from FISH staining for *F3* (pink) and immunofluorescent protein staining for SM22 (*TAGLN* protein product; green) with DAPI (gray) on the developing human intestine (n = 1 biological replicate per time point). Scale bars represent 200 μm.

(G) Spatial characterization of *PDGFRA*^{HI}/*DLL1*^{HI}/*F3*^{HI} and *GPX3*^{HI} mesenchymal cells using FISH in the developing human intestine. Multiplexed FISH/IF for *F3*, *PDGFRa*, *DLL1*, *NPY*, and *GPX3* (pink or green) was counterstained with DAPI (gray) and, in one case, ECAD (blue). Representative data are shown for n = 1 biological replicate aged 132 days for *DLL1*/*F3*, *NPY*/*F3*, and *NPY*/*GPX3*; n = 2 biological replicates for a *PDGFRA*/*F3* 120-day specimen are shown. The white dotted line roughly defines the epithelial-mesenchymal boundary Scale bars represent 25 μm.

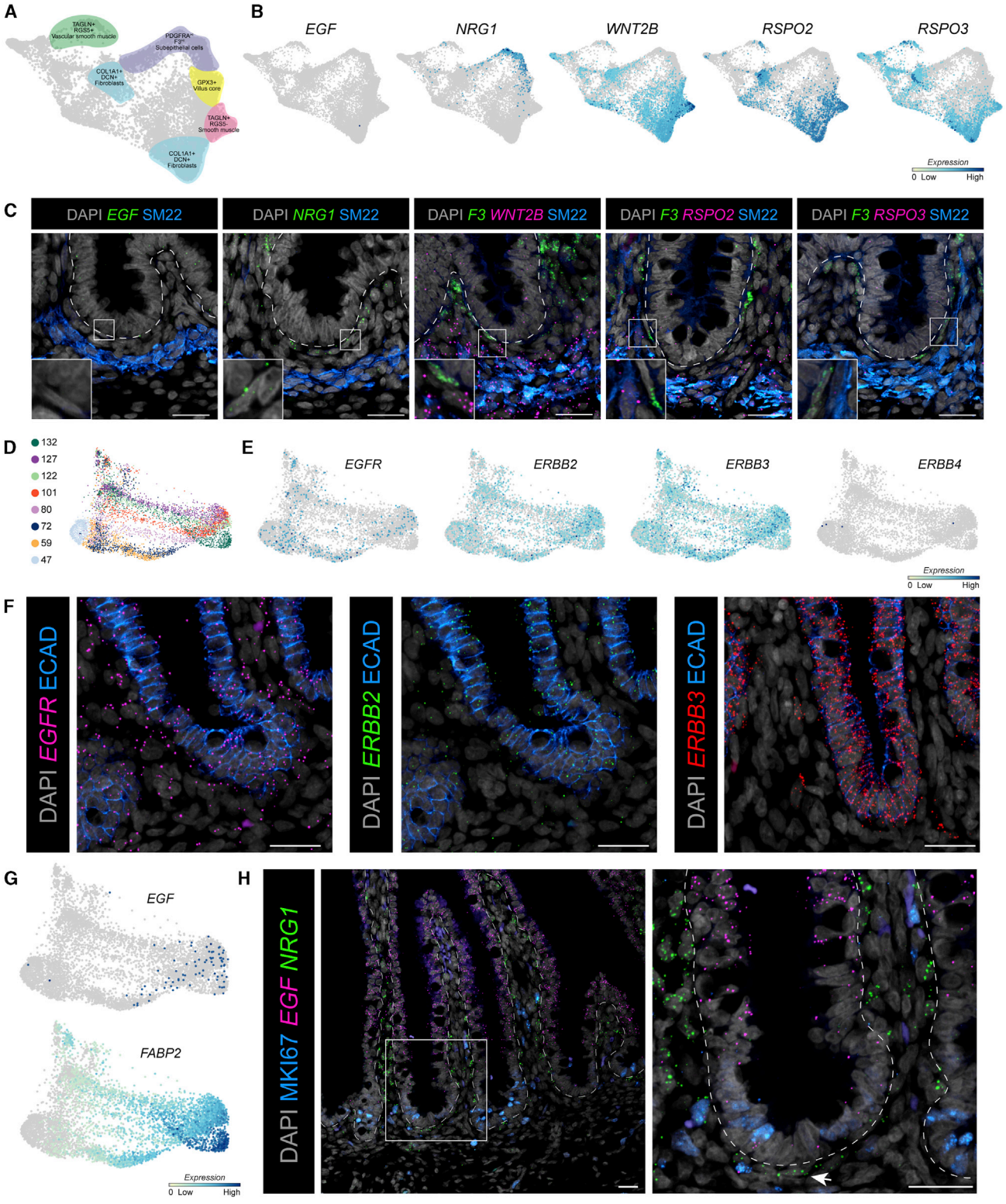

Figure 2. Interrogating Stem Cell Niche Factors in the Developing Human Intestine

(A) Summary schematic annotating the approximate expression domains of several mesenchymal subpopulations on the force-directed layout as identified in Figure 1E and Figure S1D.

(B) Feature plots of several individual ISC niche factors, including *EGF*, *NRG1*, *WNT2B*, *RSPO2*, and *RSPO3*, in mesenchymal cells at all time points profiled.

(legend continued on next page)

Mesenchymal Cell Lineages Emerge across Developmental Time

Force-directed layouts following Harmony implementation suggested that different mesenchymal cell populations emerge across developmental time. For example, *F3*^{HI}/*PDGFRA*^{HI} cells emerged after approximately 59 days, whereas *GPX3*^{HI}/*F3*^{LO}/*PDGFRA*^{LO} and *TAGLN*^{HI}/*RGS5*$^{-}$ smooth muscle cells emerge after approximately 80 days. To corroborate the scRNA-seq analysis, we used a combinatorial staining approach, utilizing multiplexed FISH and IF to examine *F3* mRNA and SM22, the protein product of the *TAGLN* gene (Figure 1F). We found that *F3* was not expressed at 59 days but was clearly expressed in the villus mesenchyme by 78 days, with expression becoming more restricted to the SECs as time progressed. Interestingly, we observed that *F3* was expressed in scRNA-seq at 59 days; however, it is possible that, because fetal tissue staging is an approximation, samples may be slightly older or younger than their actual labeling, explaining slight discrepancies such as this. SM22 was expressed in the day 59 intestine, but only in the outermost *muscularis externa* layer. SM22 expression in the *muscularis mucosa*, the layer closest to the intestinal epithelium and adjacent to the proliferative crypt domains, was first observed as poorly organized cells near the epithelium at 100 days that became more organized after this time point. Single-cell analysis and FISH/IF collectively suggest that the mesenchyme in the early fetal intestine is naive and that mesenchymal cell emergence coincides with formation of proliferative intervillus/crypt domains.

To understand how mesenchymal cell populations are organized spatially within the tissue after 100 days, we used FISH/IF and confirmed that *F3*^{HI} cells co-express *PDGFRA*, *DLL1*, and *NPY* (Figure 1G). Interestingly, *NPY* marked a subset of *F3*^{HI} SECs lining the villus but was absent from villus SECs (Figures 1G and S2D). *GPX3*^{HI}/*F3*^{LO}/*PDGFRA*^{LO} cells were most abundant within the core of intestinal villi and were observed sitting adjacent to *NPY*^{HI} cells (Figure 1E).

Identifying Putative Human ISC Niche Factors in the Developing Gut

It has been demonstrated that several niche factors allow adult and developing human and murine intestinal epithelium to be cultured *ex vivo* as organoids (Fordham et al., 2013; Fujii et al., 2018; Kraiczy et al., 2017; Sato et al., 2009, 2011b; Tsai et al., 2018). These factors often include WNT and RSPO ligands, BMP/transforming growth factor β (TGF-β) antagonists, and EGF and are based on defined growth conditions that allow expansion of intestinal epithelium *in vitro* (Sato et al., 2009, 2011b). Efforts have been made to determine more physiological niche factors for *in vitro* culture systems based on observed *in vivo* niche cues (Fujii et al., 2018); however, niche factors have not been interrogated in the developing human gut using high-resolution technologies such as scRNA-seq. To identify putative niche factors, we first determined which cells within the human fetal intestine expressed known niche factors. We observed that *F3*^{HI}/*PDGFRA*^{HI} SECs and *GPX3*^{HI}/*F3*^{LO}/*PDGFRA*^{LO} villus core cells lacked robust expression of most known niche factors (Figures 2A and 2B), whereas the WNT pathway members with the highest expression were *RSPO2*, *RSPO3*, and *WNT2B*, which are expressed in *TAGLN*^{HI}/*RGS5*$^{-}$ smooth muscle cells and *COL1A1*^{HI} fibroblasts but not expressed by *F3*^{HI}/*PDGFRA*^{HI} SECs (Figures 2A and 2B). EGF is a critical driver of proliferation in murine enteroid culture (Basak et al., 2017); however, *EGF* expression was not observed in the mesenchyme, whereas the EGF family member *NRG1* was abundant in the *F3*^{HI}/*PDGFRA*^{HI} cell population (Figures 2A and 2B). Of note, *NRG1* was one of the most robustly expressed EGF family members in the *F3*^{HI}/*PDGFRA*^{HI} cell population (Figure S3A). IF for SM22 combined with FISH for *RSPO2*, *RSPO3*, *WNT2B*, *EGF*, and *NRG1*, revealed expression patterns that were consistent with scRNA-seq data (Figures 2C and S2F).

Given the importance of EGF for *in vitro* enteroid culture, we further interrogated whether *EGF* and EGF receptors are expressed in the developing intestinal epithelium via scRNA-seq and FISH. All epithelial cells were extracted and re-clustered, and the data were visualized using a force-directed layout following application of Harmony (Figure 2D). ERBB receptors, including *EGFR*, *ERBB2*, and *ERBB3*, were broadly expressed throughout the epithelium, a finding that was confirmed by FISH, whereas *ERBB4* was not expressed (Figures 2E and 2F). Although *EGF* is not expressed in the intestinal mesenchyme (Figures 2A–2C), we observed that *EGF* is expressed in a small subset of differentiated epithelial *FABP2*^{HI} enterocytes (Figure 2G), a finding that was supported using co-FISH/IF and showed that *EGF* expression is low/absent from the proliferative crypt domain but expressed several cell diameters above the MKI67+ crypt region and throughout the villus epithelium (Figure 2D). On the other hand *NRG1* is expressed in *F3*^{HI}/*PDGFRA*^{HI} SECs adjacent to the crypt (Figures 2C, 2H, and S2B).

NRG1 Does Not Support Proliferation and Growth in Established Enteroid Cultures

Based on the expression pattern of *NRG1*, we hypothesized that it may act as an ERBB niche signaling cue and may be

(C) Multiplexed FISH for the niche factors *EGF* (green), *NRG1* (green), *WNT2B* (pink), *RSPO2* (pink), and *RSPO3* (pink), coupled with immunofluorescent protein staining of SM22 (blue), DAPI (gray), and FISH for *F3* (green) in developing human fetal crypts. Representative data are shown from n = 2 biological replicates. A 140-day specimen is shown for *EGF* and *NRG1*, and a 132-day specimen is shown for *RSPO2*, *RPSO3*, and *WNT2B*. Lower-magnification images for all panels are presented in Figure S2.

(D) Following application of Harmony to epithelial cells from all time points, force-directed layout illustrates the relationship among time points. Cells are colored by sample identity (days post conception).

(E) Feature plots of *EGFR*, *ERBB2*, *ERBB3*, and *ERBB4* plotted onto the force-directed layout presented in (D).

(F) FISH staining in developing human fetal crypts for *EGFR* (pink), *ERBB2* (green), and *ERBB3* (red), coupled with immunofluorescent staining for ECAD (blue) and DAPI (gray). Representative data are shown from n = 1 132-day biological specimen. Lower-magnification images for all panels are presented in Figure S2.

(G) Feature plots of *EGF* and the enterocyte marker *FABP2* plotted onto the force-directed layout presented in (D).

(H) Representative images of multiplexed FISH for *EGF* (pink) and *NRG1* (green), coupled with immunofluorescent protein staining of MKI67 (blue) and DAPI (gray) (n = 1 132-day human fetal intestine). The white dotted line roughly defines the epithelial-mesenchymal boundary. Scale bars represent 25 μm.

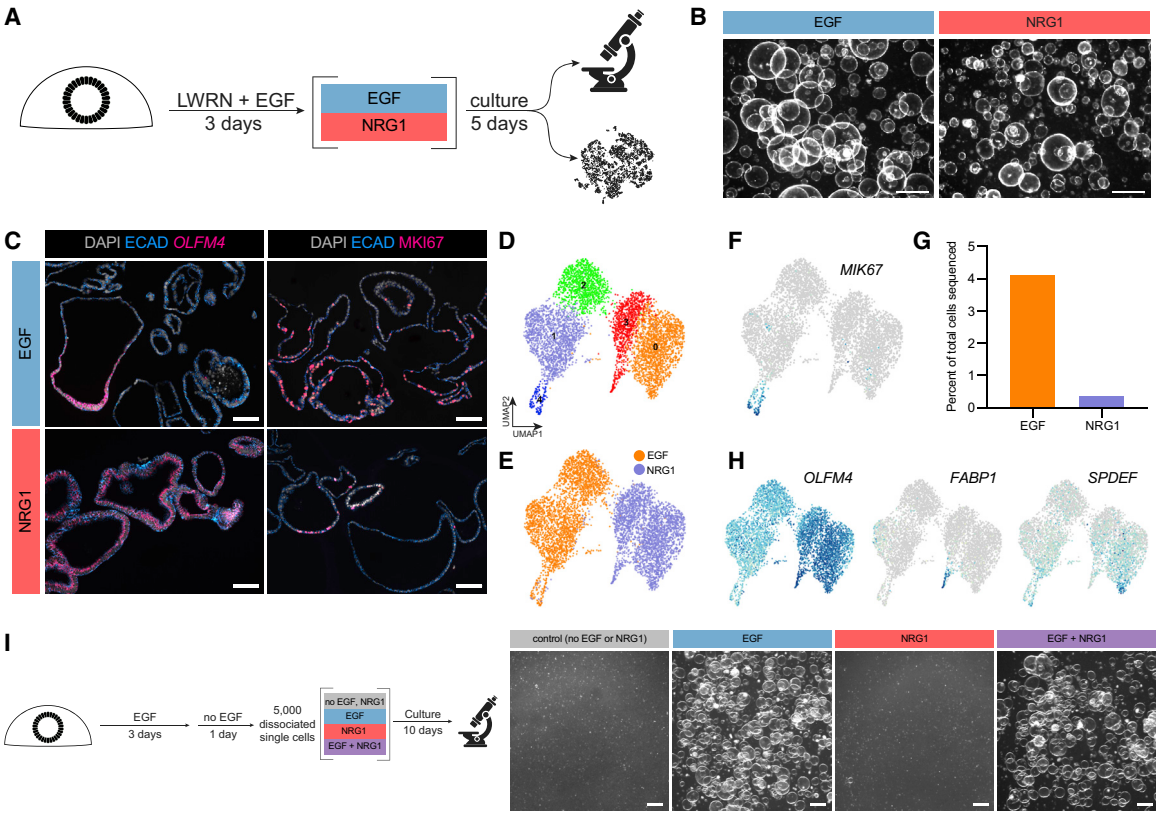

Figure 3. NRG1 Does Not Support Proliferation and Growth of Established Enteroid Lines

(A) Experimental schematic for the data presented.

(B) Representative stereomicroscopy images after 5 days of growth in the presence of EGF (100 ng/mL) or NRG1 (100 ng/mL). Scale bars represent 500 μm. Representative data are shown from n = 2 biological replicates; a 142-day fetal sample is shown.

(C) Representative images of FISH staining for *OLFM4* (pink) or immunofluorescent protein staining for MKI67 (pink), coupled with ECAD (blue) and DAPI (gray), in enteroids grown in EGF (100 ng/mL) or NRG1 (100 ng/mL). Representative data are shown from n = 2 biological replicates; a 142-day fetal sample is shown. Scale bars represent 100 μm.

(D) UMAP embedding of enteroid scRNA-seq data (5,509 cells total) demonstrating the 5 precited clusters (n = 1 biological sample sequenced, 142-day fetal sample).

(E) UMAP embedding of enteroid scRNA-seq data colored by culture condition (EGF, 2,789 cells; NRG1, 2,720 cells).

(F) Feature plot of *MKI67*, illustrating that most proliferating cells are within cluster 4.

(G) Bar chart depicting the percentage of cells in cluster 4 from each treatment group.

(H) Feature plots demonstrating the expression of the stem cell marker *OLFM4*, the secretory progenitor marker *SPDEF*, and the enterocyte marker *FABP1*.

(I) Experimental schematic for enteroid formation assays (left) and stereoscope images of enteroids after single-cell passaging and 10-day growth without EGF-family ligands (control) or in the presence of EGF (100 ng/mL), NRG1 (100 ng/mL), or EGF and NRG1 (100 ng/mL each). Representative data are shown from n = 2 biological replicates; a 142-day fetal sample is shown). Scale bars represent 500 μm.

physiologically relevant *in vitro* based on its localization and proximity to ISCs within the developing intestine *in vivo*. To interrogate the effects of NRG1 and EGF on the intestinal epithelium, we split established human fetal duodenum-derived epithelium-only intestinal enteroids (established from a 142-day specimen) in culture using standard growth conditions (WNT3A/RSPO3/NOG plus EGF; STAR Methods) into two groups. One group of enteroids was cultured in standard medium with EGF (100 ng/mL), and the other was grown without EGF and was instead supplemented with NRG1 (100 ng/mL) (Figure 3A). Following growth for 5 days in EGF or NRG1, enteroids did not appear phenotypically different (Figure 3B). Upon interrogation using IF and FISH, we observed that EGF-grown cultures had *OLFM4*+ and *OLFM4*− enteroids and that enteroids in this group were highly proliferative based on MKI67 staining (Figure 3C). NRG1-treated enteroids appeared to have more uniform *OLFM4* expression but also had fewer KI67+ cells per field of view. To more closely interrogate these differences, each group was subjected to scRNA-seq to investigate transcriptional differences. To reduce any chances of batch effect, all processing for single-cell sequencing for these groups was carried out at the same time in parallel, libraries were prepared in parallel, and samples were sequenced on the same lane (see STAR Methods for details). Despite varying only EGF or NRG1 in the culture, we observed a difference in gene expression between the two groups, as visualized in UMAP plots illustrated by nearly completely independent clustering of cells by culture medium composition (Figures 3D and 3E). The exception to this was cluster 4, which expressed proliferation markers (*MKI67* and *TOP2A*) and had a contribution

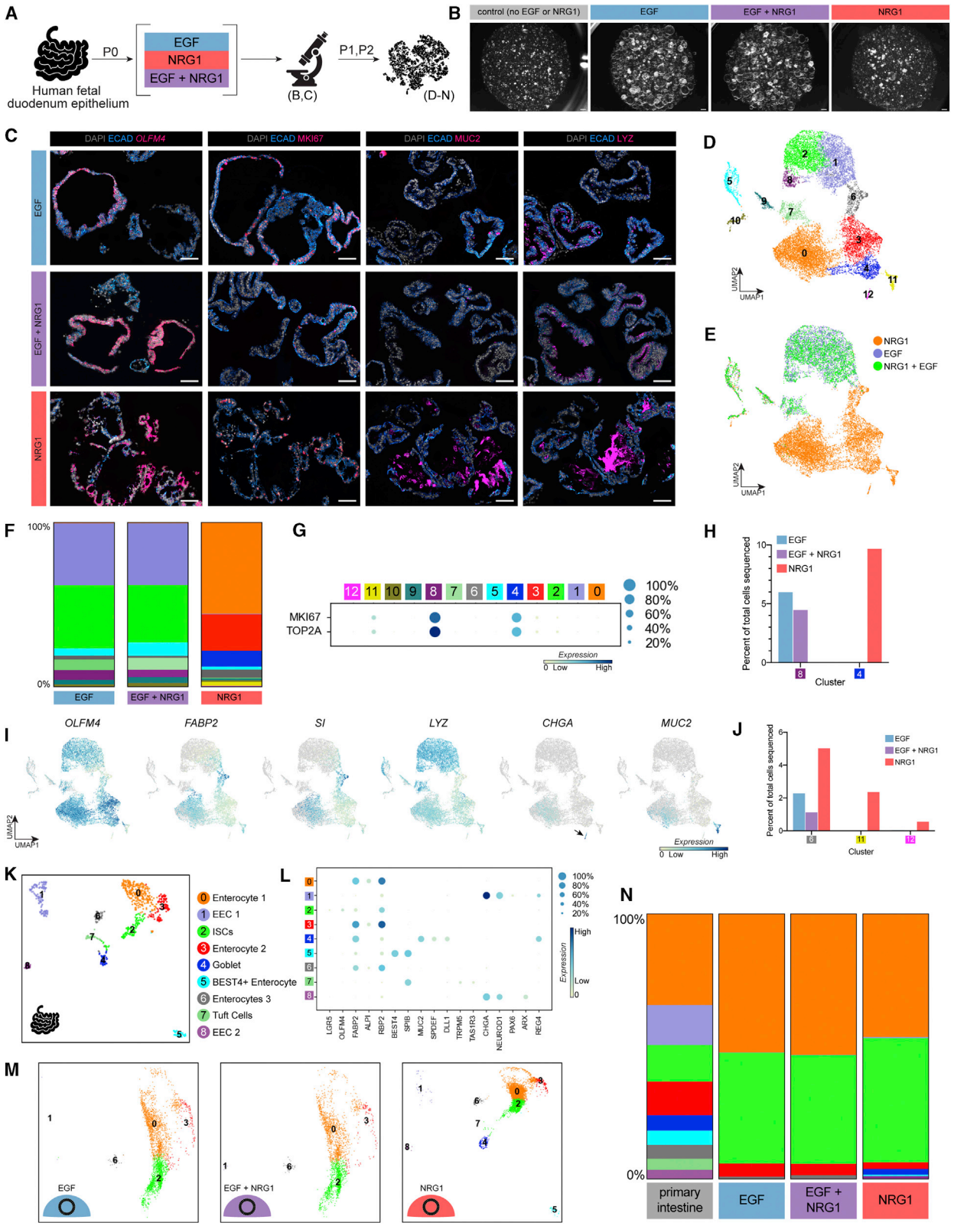

Figure 4. Establishment of New Enteroid Lines in NRG1 Increases Cell Type Diversity *In Vitro*

(A) Experimental schematic. Enteroids were established from 132-day (B and C) or 105-day (D–J) human fetal specimens in the presence of EGF (100 ng/mL), NRG1 (100 ng/mL), and EGF (100 ng/mL) and NRG1 (100 ng/mL) or without any EGF or NRG1. Representative data are shown from n = 4 biological replicates in total: 74, 101, 105, and 132 days.

(legend continued on next page)

from both samples (Figures 3E and 3F). Cluster 4 appeared to have a higher number of cells from the EGF-grown enteroids, and, proportionally, ~4% (115 of 2,789) of cells from the EGF-treated enteroids were in this cluster, whereas less than 0.5% (10 of 2,720) of cells from the NRG1-treated enteroids were in this cluster (Figure 3G). These data support the MKI67 IF staining, suggesting that NRG1 had reduced proliferation. Enteroids from both groups broadly expressed *OLFM4*, although it appeared that expression levels were slightly higher when grown in NRG1, suggesting that these samples generally had little heterogeneity and were largely comprised of undifferentiated stem cells (Figure 3H). Consistent with this notion, differentially expressed genes associated with each cluster did not include genes canonically associated with differentiated cell types (Table S1). We did note that a subset of cells in the NRG1 clusters expressed the enterocyte marker *FAPB1* (Guilmeau et al., 2007) and a subset expressed the secretory progenitor marker *SPDEF* (Gregorieff et al., 2009; Noah et al., 2010; Figure 3H). These data suggest that some cells in the NRG1 cultures may be in the early stages of differentiation; however, the expression patterns were not sufficiently different to form distinct clusters.

To functionally evaluate the observation that proliferation was reduced in NRG1-treated enteroids, we bulk-passaged enteroids and then allowed them to expand for 3 days under standard (EGF, 100 ng/mL) growth conditions. We then removed EGF for 24 h, dissociated enteroids into a single-cell suspension, and plated 5,000 cells per droplet of Matrigel. Immediately upon seeding single cells, we added standard growth medium without EGF (control), with EGF (100 ng/mL) only, with NRG1 (100 ng/mL) only, or with NRG1 (100 ng/mL) and EGF (100 ng/mL) (Figure 3I). As expected, we observed robust re-establishment of enteroids after 10 days under the standard EGF condition. In contrast, we observed almost no enteroid recovery in the control and NRG1-only supplemented cultures, whereas this growth defect was rescued under the NRG1 plus EGF condition (Figure 3I). These functional results further suggest that EGF enhances proliferation relative to NRG1 in established enteroid cultures.

Long-Term Enteroid Growth in NRG1 Is Associated with Increased Epithelial Diversity *In Vitro*

The previous experiment was conducted with enteroids that had been established and expanded in long-term culture with EGF, and the experimental data (Figure 3) suggested that these cultures were highly dependent on EGF for proliferation. To determine the effects of different EGF family members on establishment and long-term growth of enteroids, we cultured freshly isolated intestinal crypts under standard growth conditions (WNT3A/RSPO3/NOG; STAR Methods) without EGF/NRG1 (control), with EGF (100 ng/mL), with NRG1 (100 ng/mL), or with a combination of EGF and NRG1 (100 ng/mL each) (Figure 4A). We used these cultures to carry out long-term passaging, imaging, quantitative enteroid formation assays, and scRNA-seq (Figures 4A and S4). Enteroids were established successfully under all conditions (Figure 4B). All conditions successfully underwent serial passaging, with the exception of the controls (no EGF/NRG1), which failed to expand beyond initial plating (passage 0 [P0]). To determine the effects of different growth conditions on enteroid formation ability, we performed a quantitative single-cell passaging assay on surviving cultures at P2 (Figures S4B and S4C). To do this, we dissociated the three treatment groups into single cells and plated 1,000 single cells (Figure S4B) per droplet of Matrigel, allowed cultures to grow for 11 days, and quantified the number of recovered enteroids (Figure S4C). All groups re-established enteroids, albeit with low efficiency, and there was no difference in enteroid formation efficiency between the EGF and NRG1 groups.

Examining all three groups that remained after passaging (EGF, NRG1, and EGF/NRG1) by FISH or IF revealed that *OLFM4* was expressed under all conditions, and MKI67 did not appear different per field of view (Figure 4C). The NRG1-only group appeared to have more MUC2 staining within the enteroid lumen, whereas both groups that included EGF (EGF only and NRG1/EGF) had widespread LYZ expression within the epithelial cells (Figure 4C).

Given the different IF staining patterns of MUC2 and LYZ observed when comparing treatment groups (Figure 4E), we interrogated the cellular makeup and molecular signatures of these

(B) Representative stereoscope images of enteroids under each condition 8 days after placing isolated epithelium in Matrigel with growth factors. Scale bars represent 1 mm.
(C) Representative images of FISH for *OLFM4* (pink) or immunofluorescent protein staining for MKI67 (pink), MUC2 (pink), LYZ (pink), ECAD (blue), and DAPI (gray) in enteroids after P0, 11 days of growth in the presence of EGF, NRG1, or EGF and NRG1. Scale bars represent 100 μm.
(D–J) scRNA-seq was performed on enteroids under EGF, NRG1, and dual EGF/NRG1 conditions after P1, 11 days of *in vitro* growth (n = 1 biological sample sequenced, 105-day fetal sample).
(D) UMAP embedding of 13,205 enteroid cells colored by cluster identity.
(E) UMAP embedding of enteroid cells colored by sample identity (EGF, 3,262 cells; NRG1, 7,350 cells; EGF/NRG1, 2,593 cells).
(F) Bar charts depicting the cell type abundance (percentage of total cells sequenced) for each condition. The colors in the graph correspond to (D).
(G) Dot plots for the proliferation markers *MKI67* and *TOP2A*. Both markers were enriched in clusters 4 and 8.
(H) Bar chart depicting the proportion of cells sequenced that map to proliferative clusters (cluster 4 or 8) under each condition.
(I) Feature plots for intestinal epithelial lineages include ISCs (*OLFM4*; clusters 0, 1, 2, 3, 4, and 8), enterocytes (*FABP2* and *SI*; cluster 6), EECs (*CHGA*; cluster 12), and goblet cells (*MUC2*; cluster 11). *LYZ* was broadly expressed across all enteroids conditions.
(J) Bar chart depicting the proportion of cells sequenced for each condition present in cluster 6 (enterocytes), cluster 12 (EECs), and cluster 11 (goblet cells).
(K) Epithelial cells (828 cells) from primary intestine specimens (n = 4; 101, 122, 127, and 132 days) were extracted computationally, re-clustered, and visualized using UMAP.
(L) Cluster identities were assigned based on expression of canonical lineage markers (see Table S3 for differentially expressed genes in each cluster).
(M) The *Ingest* function was used to map enteroids derived in the presence of EGF (100 ng/mL), NRG1 (100 ng/mL), or EGF and NRG1 (100 ng/mL) onto the primary intestinal epithelium reference presented in (K).
(N) The abundance of cells mapping to each of the 9 clusters identified in the *in vivo* intestinal epithelium was determined for the primary intestinal epithelium and for enteroids in each treatment group. The colors in the graph correspond to (K).

enteroids using scRNA-seq. We sequenced 3,262 cells grown in EGF (100 ng/mL), 7,350 cells grown in NRG1 (100 ng/mL), and 2,593 cells grown in NRG1 and EGF (100 ng/mL each). UMAP dimensional reduction showed that NRG1-treated enteroids clustered distinctly from the EGF-only enteroids and suggested that NRG1/EGF enteroids shared a high degree of molecular similarity with EGF-only enteroids because these samples overlapped in the clustering (Figures 4E and 4F). Examining the cluster distribution for each sample, it was evident that EGF and EGF/NRG1 enteroids contributed to the same clusters (clusters 1, 2, 7 and 8), whereas NRG1 contributed to many distinct clusters (0, 3, 4, 11, and 12) (Figure 4F). Upon interrogation of genes associated with various clusters (Table S2), proliferation genes were associated with two clusters: cluster 4 (NRG1) and cluster 8 (EGF and EGF/NRG1) (Figures 4G and 4H). Several clusters expressed the stem cell marker *OLFM4* (EGF and EGF/NRG1: clusters 1, 2, and 8; NRG1: clusters 0, 3, and 4). Cluster 6 had a contribution from all 3 groups and expressed enterocyte genes (*SI* and *FAPB2).* Unique to the NRG1 grown enteroids, cluster 11 expressed genes associated with secretory and goblet cells (*MUC2*), and cluster 12 expressed genes associated with enteroendocrine cells (*CHGA*) (Figure 4I). We also interrogated *LYZ* expression given our IF staining results. *LYZ* was expressed at higher levels in EGF and NRG1/EGF enteroids, as suggested by IF; however, low-level expression was also observed broadly in the NRG1 treatment group (Figure 4I). LYZ is canonically associated with Paneth cells; however, the fetal intestine does not possess Paneth cells until 21 weeks after conception (Elmentaite et al., 2020; Finkbeiner et al., 2015). Given that the enteroids used here were generated from specimens earlier than 21 weeks (replicate experiments utilized day 105 and day 135 specimens), it is unlikely that *LYZ* expression is associated with Paneth cells. These data show that EGF and NRG1 can promote long-term survival of freshly established enteroids but that they have different effects on gene expression and cellular diversity.

Mapping to an Intestinal Reference Reveals Cellular Heterogeneity in Enteroids

To further interrogate cellular heterogeneity in enteroids grown in EGF, NRG1, and EGF/NRG1, we used human fetal epithelium as a high-dimensional search space to determine the potential correspondence of enteroids and their *in vivo* counterparts. To do this, we implemented the *Ingest* function (Wolf et al., 2018), which uses an annotated reference dataset that captures the biological variability of interest and projects new data onto the reference. We defined the major epithelial cell populations in the human fetal intestine using the four samples that were older than 100 days (101–132 days). These samples were chosen based on the force-directed layouts following Harmony augmentation, which suggested that major changes in development/differentiation were not taking place across these times (Figures 1 and 2). We defined 9 epithelial cell types based on published data (Table S3), including ISCs (cluster 2: *LGR5* and *OLFM4*), enterocytes (clusters 0 and 3: *FABP2*, *ALPI*, and *RBP2*; Haber et al., 2017), BEST4+ enterocytes (cluster 5: *BEST4* and *SPIB*; Elmentaite et al., 2020; Parikh et al., 2019), goblet cells and goblet cell precursors (cluster 4: *MUC2*, *SPDEF*, and *DLL1*; Okamoto et al., 2009), tuft cells (cluster 7: *TRPM5*, *TAS1R3*, and *SPIB*; van Es et al., 2019; Howitt et al., 2020; Kaske et al., 2007), enteroendocrine cells (EECs; clusters 1 and 8: *CHGA*, *NEUROD1*, *PAX6*, *ARX*, and *REG4*; Beucher et al., 2012; Du et al., 2012; Gehart et al., 2019; Haber et al., 2017 (Figures 4K and 4L). We then used Ingest to map enteroids grown in EGF, EGF/NRG1, or NRG1 onto the *in vivo* epithelium (Figure 4M), determined the proportion of cells that mapped to each *in vivo* cell type, and compared this with the distribution of cells seen in the primary intestine (Figure 4N). EGF and EGF/NRG1 samples shared similar distribution patterns, with the majority of cells from both conditions mapping to ISCs and enterocytes (Figures 4M and 4N). NRG1-treated enteroids mapped to all cell types, including goblet cells (cluster 4), CHGA+ EECs (cluster 8), tuft cells (cluster 7), and BEST4+ enterocytes (cluster 5), that were not present in EGF- or EGF/NRG1-grown enteroids in this analysis (Figures 4M and 4N). These results further support that NRG1-grown enteroids have enhanced cellular differentiation relative to enteroids grown in EGF.

DISCUSSION

Subepithelial Niche Cells in the Developing Human Intestine

Based on scRNA-seq and confirmatory FISH, we observed that *WNT2B*, *RSPO2*, and *RSPO3* are expressed in the *muscularis mucosa* in the human fetal intestine as well as in cells more broadly defined as fibroblasts. However, the *muscularis mucosa* is a muscle layer that is located closest to proliferative domain of the intestine. This is a unique finding compared with recent single-cell studies in the adult human colon and compared with findings in the mouse. In the adult human colon, a source of WNT and RSPO external to the muscular mucosa has been identified as *WNT2B/RSPO3*+ fibroblasts (Smillie et al., 2019), whereas in mice, WNT and RSPO ligands are expressed in cells that were recently coined "trophocytes" and in PDGRFA^{LO} stroma cells in the small intestine (McCarthy et al., 2020). In addition, identification of the *Foxl1*+ telocyte was a major advance in elucidating the cells and sources of many niche factors in the murine ISC niche (Aoki et al., 2016; Shoshkes-Carmel et al., 2018). When *Foxl1*+ cells are genetically ablated, the crypt collapses; however, recent single-cell studies have shown that telocytes are not a major source of WNT or RSPO ligands (Kim et al., 2020; McCarthy et al., 2020), and others have demonstrated that non-telocytes express RSPO3 (Greicius et al., 2018; Shoshkes-Carmel et al., 2018). Single-cell studies in humans have initially focused on the colon (Kinchen et al., 2018; Smillie et al., 2019), so it remains to be seen whether there is a unique expression pattern in the adult human small intestine and/or whether there are changes in the cellular sources for *WNT2B* and *RSPO2/3* as development progresses. However, because the gross anatomical structure of the intestine observed in the fetal stages starting at 100 days post conception and onward is maintained into adulthood (i.e., crypt-villus axis, muscle layers), it is possible that there are dramatic differences across species and regions of the gut for the major niche cells.

In the current work, we identify an SEC that lines the entire crypt-villus axis, marked by high levels of *DLL1*, *F3*, and *PDGFRA* expression. These cells can be further sub-divided using the marker *NPY*, which is expressed in the villus (*NPY/DLL1/F3)* but not the crypt. Within the *F3* transcriptional signature, we also observed robust expression of *FRZB* and *SOX6*, which have been described

previously in the human colon as an SEC population that expresses several WNT family members (*WNT5A* and *WNT5B*) and several BMP family members (*BMP2* and *BMP5*) (Kinchen et al., 2018). Thus, although the focus of the current manuscript is on EGF family members, it is likely that the niche signaling role of $DLL1^{HI}/F3^{HI}$ is more complex and may involve secretion of activators and inhibitors of several other signaling pathways.

Establishing Signaling Gradients along the Crypt-Villus Axis

Although difficult or impossible to test in human tissue, one can speculate that the robust levels of *EGF* expressed in the villus epithelium coupled with *NRG1* expression in SECs along the crypt-villus axis help to establish, in effect, a gradient of EGF/NRG1 signaling by differential receptor binding/dimerization in different domains. For example, high *NRG1* is expressed in crypt-associated SECs, with low/no *EGF* being expressed in the in the crypt domain, whereas NRG1 and lower levels of EGF are present in the putative TA zone. Finally, high NRG1 and high EGF are likely present in the villus, based on FISH data, but this area would also have the lowest levels of RSPO and WNT, given our localization data showing that *RSPO* and *WNT* ligands are low/absent in the villus core. Given these spatial differences, it is interesting to speculate that EGF normally acts as a differentiation factor in the absence of WNT signaling. However, the interplay between WNT signaling and EGF signaling is likely to intersect with other signaling pathways as well, given that gradients of BMP signaling are also established along the crypt-villus axis (McCarthy et al., 2020).

Future work may focus on how dose-dependent gradients from multiple signaling pathways intersect with one another to finely tune human stem cell maintenance and differentiation, and it is clear that there is still much to be understood about the human niche. In mice, a minimal set of niche factors is able to maintain intestinal enteroids in a homeostatic state, with stem cells and differentiated cells taking on proper crypt-villus organization (Sato et al., 2009). This organization is dependent on Paneth cell differentiation and secretion of WNT ligands, allowing crypts to bud into their own spatial domains in enteroids (Sato et al., 2011a; Serra et al., 2019). However, such a homeostatic state, which allows stem cell maintenance and differentiation, has not been achieved in human enteroid cultures, and to date, human enteroids are largely maintained in a stem cell state, are switched to differentiation medium to allow cytodifferentiation, or require engineered scaffolds and growth factor gradients to establish crypt-villus domains (Dame et al., 2018; Sato et al., 2011b; VanDussen et al., 2015; Wang et al., 2017). Here we show that EGF signaling members may play a role in such a homeostatic state, given our findings that NRG1 permits cytodifferentiation while maintaining stem cells *in vitro*; however, it was clear that neither EGF- nor NRG1-grown enteroids possessed crypt-villus architecture.

Our data reveal that the human fetal ISC niche is composed of multiple cellular sources and highlights a unique role for different ligands from the EGF family. The resources we provide here lay the groundwork to further interrogate cellular relationships in the human fetal intestine, provide an important benchmark for *in vitro* experiments, and will inform additional methods to generate more robust and physiological culture conditions.

Limitations of Study

Shortly after initial submission of this manuscript, the world was gripped by a global pandemic caused by the severe acute respiratory syndrome coronavirus 2 (SARS-CoV-2) virus. This forced massive shutdowns of biomedical research across the United States and across the world for many months, significantly affecting our ability to carry out new experiments. Fortunately, much of the data for this manuscript were on hand and allowed us to perform additional computational analyses, and follow-up studies also relied on archival tissue in the laboratory prior to shutdown. Nonetheless, there were some limitations imposed by the pandemic; access to new tissue for this study was effectively stopped, and this prevented plans to isolate different mesenchymal cell populations (i.e., $F3^{HI}$/$PDGFRA^{HI}$) to directly test the function of these cells to support enteroids *in vitro*. Another clear limitation in this study (irrespective of the global pandemic) is the limited ability to carry out experiments in human tissue. Our result in Figure 1, based on force-directed layouts following implementation of Harmony, suggests that there are lineage trajectories of emerging mesenchymal cell populations over time. For example, our data suggest that cell trajectories change dramatically and diversify over time (Figures 1D and 1E); however, without the ability to carry out *bona fide* lineage tracing, inferred cell trajectories should be interpreted with caution. Similarly, the temporal resolution of our data, with datasets being 1 week or more apart, prohibits certain types of analyses, such as RNA velocity (La Manno et al., 2018), which would require much higher temporal resolution to draw meaningful inferences between the time points.

STAR★METHODS

Detailed methods are provided in the online version of this paper and include the following:

- KEY RESOURCES TABLE
- RESOURCE AVAILABILITY
  - Lead Contact
  - Materials Availability
  - Data Code and Availability
- EXPERIMENTAL MODEL AND SUBJECT DETAILS
  - Isolating, establishing and maintaining human fetal enteroids
  - Media composition
  - Human subjects
- METHOD DETAILS
  - Experimental design of enteroid cultures
  - Single cell dissociation
  - Single cell library preparation and transcriptome alignment
  - Primary tissue collection, fixation and paraffin processing
  - Enteroid collection, fixation and paraffin processing
  - Multiplex Fluorescent *In Situ* Hybridization (FISH) and immunofluorescence (IF)
- QUANTIFICATION AND STATISTICAL ANALYSIS
  - Single-cell *in silico* analysis

SUPPLEMENTAL INFORMATION

Supplemental Information can be found online at https://doi.org/10.1016/j.stem.2020.11.008.

ACKNOWLEDGMENTS

This work was supported by the Intestinal Stem Cell Consortium (U01DK103141 to J.R.S.), a collaborative research project funded by the National Institute of Diabetes and Digestive and Kidney Diseases (NIDDK) and the National Institute of Allergy and Infectious Diseases (NIAID). This work was also supported by the NIAID Novel Alternative Model Systems for Enteric Diseases (NAMSED) consortium (U19AI116482 to J.R.S.), by a Chan Zuckerberg Initiative Seed Network grant (to J.R.S., B.T., and J.G.C.), and by the University of Michigan Center for Gastrointestinal Research (UMCGR) (NIDDK 5P30DK034933). K.W. is supported by NIDDK R01KD121166. I.G. and the University of Washington Laboratory of Developmental Biology were supported by NIH award 5R24HD000836 from the Eunice Kennedy Shriver National Institute of Child Health and Human Development (NICHD). M.C. was supported by the Training Program in Organogenesis (NIH-NICHD T32 HD007505). E.M.H. was supported by a Training in Basic and Translational Digestive Sciences training grant (NIH-NIDDK 5T32DK094775), a Cellular Biotechnology Training Program training grant (NIH-NIGMS 2T32GM008353), and a Ruth L. Kirschstein Predoctoral Individual National Research Service Award (NIH-NHLBI F31HL146162).

We thank Judy Opp and the University of Michigan Advanced Genomics Core for their expertise regarding operating the 10X Chromium single-cell capture platform and sequencing. We would also like to thank the University of Michigan Microscopy Core for providing access to confocal microscopes and image analysis software and The University of Washington Laboratory of Developmental Biology staff.

AUTHOR CONTRIBUTIONS

M.C. and J.R.S. conceived the study. J.R.S. supervised the research. A.W., E.M.H., Y.-H.T., and M.C. developed tissue dissociation methods and generated single-cell RNA sequencing data. M.C., J.H.W., Q.Y., B.T., and J.G.C. performed computational analyses. E.M.H., M.C., J.H.W., Q.Y., B.T., J.G.C., and J.R.S. interpreted computational results. E.M.H., K.D.W., C.W.S., and C.J.C. performed and analyzed FISH experiments and imaging. Y.-H.T. and A.W. performed enteroid experiments. Y.-H.T., A.W., and E.M.H. analyzed and interpreted enteroid experiments. I.G. provided critical material resources for this work. E.M.H., M.C., and Y.-H.T. assembled figures. E.M.H., M.C., and J.R.S. wrote the manuscript. E.M.H., Y.-H.T., A.W., K.D.W., J.H.W., C.J.C., and M.C. contributed methods. All authors edited, read, and approved the manuscript.

DECLARATION OF INTERESTS

The authors declare no competing interests.

Received: January 31, 2020
Revised: August 27, 2020
Accepted: November 11, 2020
Published: December 4, 2020

REFERENCES

Aoki, R., Shoshkes-Carmel, M., Gao, N., Shin, S., May, C.L., Golson, M.L., Zahm, A.M., Ray, M., Wiser, C.L., Wright, C.V.E., and Kaestner, K.H. (2016). Foxl1-expressing mesenchymal cells constitute the intestinal stem cell niche. Cell. Mol. Gastroenterol. Hepatol. *2*, 175–188.

Basak, O., Beumer, J., Wiebrands, K., Seno, H., van Oudenaarden, A., and Clevers, H. (2017). Induced Quiescence of Lgr5+ Stem Cells in Intestinal Organoids Enables Differentiation of Hormone-Producing Enteroendocrine Cells. Cell Stem Cell *20*, 177–190.e4.

Becht, E., McInnes, L., Healy, J., Dutertre, C.A., Kwok, I.W.H., Ng, L.G., Ginhoux, F., and Newell, E.W. (2018). Dimensionality reduction for visualizing single-cell data using UMAP. Nat. Biotechnol. *37*, 38–47.

Beucher, A., Gjernes, E., Collin, C., Courtney, M., Meunier, A., Collombat, P., and Gradwohl, G. (2012). The homeodomain-containing transcription factors Arx and Pax4 control enteroendocrine subtype specification in mice. PLoS ONE *7*, e36449.

Capeling, M.M., Czerwinski, M., Huang, S., Tsai, Y.-H., Wu, A., Nagy, M.S., Juliar, B., Sundaram, N., Song, Y., Han, W.M., et al. (2019). Nonadhesive Alginate Hydrogels Support Growth of Pluripotent Stem Cell-Derived Intestinal Organoids. Stem Cell Reports *12*, 381–394.

Capeling, M., Huang, S., Mulero-Russe, A., Cieza, R., Tsai, Y.H., Garcia, A., and Hill, D.R. (2020). Generation of small intestinal organoids for experimental intestinal physiology. Methods Cell Biol. *159*, 143–174.

Chin, A.M., Hill, D.R., Aurora, M., and Spence, J.R. (2017). Morphogenesis and maturation of the embryonic and postnatal intestine. Semin. Cell Dev. Biol. *66*, 81–93.

Cruz-Acuña, R., Quirós, M., Farkas, A.E., Dedhia, P.H., Huang, S., Siuda, D., García-Hernández, V., Miller, A.J., Spence, J.R., Nusrat, A., and García, A.J. (2017). Synthetic hydrogels for human intestinal organoid generation and colonic wound repair. Nat. Cell Biol. *19*, 1326–1335.

Dame, M.K., Attili, D., McClintock, S.D., Dedhia, P.H., Ouillette, P., Hardt, O., Chin, A.M., Xue, X., Laliberte, J., Katz, E.L., et al. (2018). Identification, isolation and characterization of human LGR5-positive colon adenoma cells. Development *145*, dev153049.

Dedhia, P.H., Bertaux-Skeirik, N., Zavros, Y., and Spence, J.R. (2016). Organoid Models of Human Gastrointestinal Development and Disease. Gastroenterology *150*, 1098–1112.

Du, A., McCracken, K.W., Walp, E.R., Terry, N.A., Klein, T.J., Han, A., Wells, J.M., and May, C.L. (2012). Arx is required for normal enteroendocrine cell development in mice and humans. Dev. Biol. *365*, 175–188.

Elmentaite, R., Ross, A., James, K., Ortmann, D., Gomes, T., Roberts, K., Nayak, K., Tuck, L., Bayraktar, O.A., Heuschkel, R., et al. (2020). Single-cell sequencing of developing human gut reveals transcriptional links to childhood Crohn's disease. bioRxiv. https://doi.org/10.1101/2020.02.06.937110.

Finkbeiner, S.R., Hill, D.R., Altheim, C.H., Dedhia, P.H., Taylor, M.J., Tsai, Y.-H., Chin, A.M., Mahe, M.M., Watson, C.L., Freeman, J.J., et al. (2015). Transcriptome-wide Analysis Reveals Hallmarks of Human Intestine Development and Maturation In Vitro and In Vivo. Stem Cell Reports *4*, 1140–1155.

Fleming, S., Marioni, J., and Babadi, M. (2019). CellBender remove-background: a deep generative model for unsupervised removal of background noise from scRNA-seq datasets. bioRxiv. https://doi.org/10.1101/791699.

Fordham, R.P., Yui, S., Hannan, N.R.F., Soendergaard, C., Madgwick, A., Schweiger, P.J., Nielsen, O.H., Vallier, L., Pedersen, R.A., Nakamura, T., et al. (2013). Transplantation of expanded fetal intestinal progenitors contributes to colon regeneration after injury. Cell Stem Cell *13*, 734–744.

Fujii, M., Matano, M., Toshimitsu, K., Takano, A., Mikami, Y., Nishikori, S., Sugimoto, S., and Sato, T. (2018). Human Intestinal Organoids Maintain Self-Renewal Capacity and Cellular Diversity in Niche-Inspired Culture Condition. Cell Stem Cell *23*, 787–793.e6.

Gehart, H., van Es, J.H., Hamer, K., Beumer, J., Kretzschmar, K., Dekkers, J.F., Rios, A., and Clevers, H. (2019). Identification of Enteroendocrine Regulators by Real-Time Single-Cell Differentiation Mapping. Cell *176*, 1158–1173.e16.

Gjorevski, N., Sachs, N., Manfrin, A., Giger, S., Bragina, M.E., Ordóñez-Morán, P., Clevers, H., and Lutolf, M.P. (2016). Designer matrices for intestinal stem cell and organoid culture. Nature *539*, 560–564.

Goodlad, R.A., Wilson, T.J., Lenton, W., Gregory, H., McCullagh, K.G., and Wright, N.A. (1987). Proliferative effects of urogastrone-EGF on the intestinal epithelium. Gut *28* (*Suppl*), 37–43.

Gregorieff, A., Stange, D.E., Kujala, P., Begthel, H., van den Born, M., Korving, J., Peters, P.J., and Clevers, H. (2009). The ets-domain transcription factor

Spdef promotes maturation of goblet and paneth cells in the intestinal epithelium. Gastroenterology *137*, 1333–45.e1, 3.

Greicius, G., Kabiri, Z., Sigmundsson, K., Liang, C., Bunte, R., Singh, M.K., and Virshup, D.M. (2018). *PDGFRα*$^{+}$ pericryptal stromal cells are the critical source of Wnts and RSPO3 for murine intestinal stem cells in vivo. Proc. Natl. Acad. Sci. USA *115*, E3173–E3181.

Guilmeau, S., Niot, I., Laigneau, J.P., Devaud, H., Petit, V., Brousse, N., Bouvier, R., Ferkdadji, L., Besmond, C., Aggerbeck, L.P., et al. (2007). Decreased expression of Intestinal I- and L-FABP levels in rare human genetic lipid malabsorption syndromes. Histochem. Cell Biol. *128*, 115–123.

Haber, A.L., Biton, M., Rogel, N., Herbst, R.H., Shekhar, K., Smillie, C., Burgin, G., Delorey, T.M., Howitt, M.R., Katz, Y., et al. (2017). A single-cell survey of the small intestinal epithelium. Nature *551*, 333–339.

Haramis, A.P.G., Begthel, H., Van Den Born, M., Van Es, J., Jonkheer, S., Offerhaus, G.J.A., and Clevers, H. (2004). De Novo Crypt Formation and Juvenile Polyposis on BMP Inhibition in Mouse Intestine. Science *303*, 1684–1686.

Howitt, M.R., Cao, Y.G., Gologorsky, M.B., Li, J.A., Haber, A.L., Biton, M., Lang, J., Michaud, M., Regev, A., and Garrett, W.S. (2020). The Taste Receptor TAS1R3 Regulates Small Intestinal Tuft Cell Homeostasis. Immunohorizons *4*, 23–32.

Jacomy, M., Venturini, T., Heymann, S., and Bastian, M. (2014). ForceAtlas2, a continuous graph layout algorithm for handy network visualization designed for the Gephi software. PLoS ONE *9*, e98679.

Jardé, T., Chan, W.H., Rossello, F.J., Kaur Kahlon, T., Theocharous, M., Kurian Arackal, T., Flores, T., Giraud, M., Richards, E., Chan, E., et al. (2020). Mesenchymal Niche-Derived Neuregulin-1 Drives Intestinal Stem Cell Proliferation and Regeneration of Damaged Epithelium. Cell Stem Cell *27*, 646–662.e7.

Kaske, S., Krasteva, G., König, P., Kummer, W., Hofmann, T., Gudermann, T., and Chubanov, V. (2007). TRPM5, a taste-signaling transient receptor potential ion-channel, is a ubiquitous signaling component in chemosensory cells. BMC Neurosci. *8*, 49.

Kim, J.E., Fei, L., Yin, W.C., Coquenlorge, S., Rao-Bhatia, A., Zhang, X., Shi, S.S.W., Lee, J.H., Hahn, N.A., Rizvi, W., et al. (2020). Single cell and genetic analyses reveal conserved populations and signaling mechanisms of gastrointestinal stromal niches. Nat. Commun. *11*, 334.

Kinchen, J., Chen, H.H., Parikh, K., Antanaviciute, A., Jagielowicz, M., Fawkner-Corbett, D., Ashley, N., Cubitt, L., Mellado-Gomez, E., Attar, M., et al. (2018). Structural Remodeling of the Human Colonic Mesenchyme in Inflammatory Bowel Disease. Cell *175*, 372–386.e17.

Kraiczy, J., Nayak, K.M., Howell, K.J., Ross, A., Forbester, J., Salvestrini, C., Mustata, R., Perkins, S., Andersson-Rolf, A., Leenen, E., et al. (2017). DNA methylation defines regional identity of human intestinal epithelial organoids and undergoes dynamic changes during development. Gut *68*, 49–61.

Kretzschmar, K., and Clevers, H. (2016). Organoids: Modeling Development and the Stem Cell Niche in a Dish. Dev. Cell *38*, 590–600.

La Manno, G., Soldatov, R., Zeisel, A., Braun, E., Hochgerner, H., Petukhov, V., Lidschreiber, K., Kastriti, M.E., Lönnerberg, P., Furlan, A., et al. (2018). RNA velocity of single cells. Nature *560*, 494–498.

Martin, J.C., Chang, C., Boschetti, G., Ungaro, R., Giri, M., Grout, J.A., Gettler, K., Chuang, L.S., Nayar, S., Greenstein, A.J., et al. (2019). Single-Cell Analysis of Crohn's Disease Lesions Identifies a Pathogenic Cellular Module Associated with Resistance to Anti-TNF Therapy. Cell *178*, 1493–1508.e20.

McCarthy, N., Manieri, E., Storm, E.E., Saadatpour, A., Luoma, A.M., Kapoor, V.N., Madha, S., Gaynor, L.T., Cox, C., Keerthivasan, S., et al. (2020). Distinct Mesenchymal Cell Populations Generate the Essential Intestinal BMP Signaling Gradient. Cell Stem Cell *26*, 391–402.e5.

McInnes, L., Healy, J., Saul, N., and Großberger, L. (2018). UMAP: Uniform Manifold Approximation and Projection. J. Open Source Softw. *3*, 861.

Miyoshi, H., and Stappenbeck, T.S. (2013). In vitro expansion and genetic modification of gastrointestinal stem cells in spheroid culture. Nat. Protoc. *8*, 2471–2482.

Muhl, L., Genové, G., Leptidis, S., Liu, J., He, L., Mocci, G., Sun, Y., Gustafsson, S., Buyandelger, B., Chivukula, I.V., et al. (2020). Single-cell analysis uncovers fibroblast heterogeneity and criteria for fibroblast and mural cell identification and discrimination. Nat. Commun. *11*, 3953.

Muncan, V., Sansom, O.J., Tertoolen, L., Phesse, T.J., Begthel, H., Sancho, E., Cole, A.M., Gregorieff, A., de Alboran, I.M., Clevers, H., and Clarke, A.R. (2006). Rapid loss of intestinal crypts upon conditional deletion of the Wnt/Tcf-4 target gene c-Myc. Mol. Cell. Biol. *26*, 8418–8426.

Noah, T.K., Kazanjian, A., Whitsett, J., and Shroyer, N.F. (2010). SAM pointed domain ETS factor (SPDEF) regulates terminal differentiation and maturation of intestinal goblet cells. Exp. Cell Res. *316*, 452–465.

Nowotschin, S., Setty, M., Kuo, Y.Y., Liu, V., Garg, V., Sharma, R., Simon, C.S., Saiz, N., Gardner, R., Boutet, S.C., et al. (2019). The emergent landscape of the mouse gut endoderm at single-cell resolution. Nature *569*, 361–367.

Okamoto, R., Tsuchiya, K., Nemoto, Y., Akiyama, J., Nakamura, T., Kanai, T., and Watanabe, M. (2009). Requirement of Notch activation during regeneration of the intestinal epithelia. Am. J. Physiol. Gastrointest. Liver Physiol. *296*, G23–G35.

Ootani, A., Li, X., Sangiorgi, E., Ho, Q.T., Ueno, H., Toda, S., Sugihara, H., Fujimoto, K., Weissman, I.L., Capecchi, M.R., and Kuo, C.J. (2009). Sustained in vitro intestinal epithelial culture within a Wnt-dependent stem cell niche. Nat. Med. *15*, 701–706.

Parikh, K., Antanaviciute, A., Fawkner-Corbett, D., Jagielowicz, M., Aulicino, A., Lagerholm, C., Davis, S., Kinchen, J., Chen, H.H., Alham, N.K., et al. (2019). Colonic epithelial cell diversity in health and inflammatory bowel disease. Nature *567*, 49–55.

Pinto, D., Gregorieff, A., Begthel, H., and Clevers, H. (2003). Canonical Wnt signals are essential for homeostasis of the intestinal epithelium. Genes Dev. *17*, 1709–1713.

Polański, K., Young, M.D., Miao, Z., Meyer, K.B., Teichmann, S.A., and Park, J.-E. (2020). BBKNN: fast batch alignment of single cell transcriptomes. Bioinformatics *36*, 964–965.

Sansom, O.J., Reed, K.R., Hayes, A.J., Ireland, H., Brinkmann, H., Newton, I.P., Batlle, E., Simon-Assmann, P., Clevers, H., Nathke, I.S., et al. (2004). Loss of Apc in vivo immediately perturbs Wnt signaling, differentiation, and migration. Genes Dev. *18*, 1385–1390.

Sato, T., Vries, R.G., Snippert, H.J., van de Wetering, M., Barker, N., Stange, D.E., van Es, J.H., Abo, A., Kujala, P., Peters, P.J., and Clevers, H. (2009). Single Lgr5 stem cells build crypt-villus structures in vitro without a mesenchymal niche. Nature *459*, 262–265.

Sato, T., van Es, J.H., Snippert, H.J., Stange, D.E., Vries, R.G., van den Born, M., Barker, N., Shroyer, N.F., van de Wetering, M., and Clevers, H. (2011a). Paneth cells constitute the niche for Lgr5 stem cells in intestinal crypts. Nature *469*, 415–418.

Sato, T., Stange, D.E., Ferrante, M., Vries, R.G.J., Van Es, J.H., Van den Brink, S., Van Houdt, W.J., Pronk, A., Van Gorp, J., Siersema, P.D., and Clevers, H. (2011b). Long-term expansion of epithelial organoids from human colon, adenoma, adenocarcinoma, and Barrett's epithelium. Gastroenterology *141*, 1762–1772.

Scadden, D.T. (2006). The stem-cell niche as an entity of action. Nature *441*, 1075–1079.

Serra, D., Mayr, U., Boni, A., Lukonin, I., Rempfler, M., Challet Meylan, L., Stadler, M.B., Strnad, P., Papasaikas, P., Vischi, D., et al. (2019). Self-organization and symmetry breaking in intestinal organoid development. Nature *569*, 66–72.

Shoshkes-Carmel, M., Wang, Y.J., Wangensteen, K.J., Tóth, B., Kondo, A., Massasa, E.E., Itzkovitz, S., and Kaestner, K.H. (2018). Subepithelial telocytes are an important source of Wnts that supports intestinal crypts. Nature *557*, 242–246.

Smillie, C.S., Biton, M., Ordovas-Montanes, J., Sullivan, K.M., Burgin, G., Graham, D.B., Herbst, R.H., Rogel, N., Slyper, M., Waldman, J., et al. (2019). Intra- and Inter-cellular Rewiring of the Human Colon during Ulcerative Colitis. Cell *178*, 714–730.e22.

Spence, J.R., Mayhew, C.N., Rankin, S.A., Kuhar, M.F., Vallance, J.E., Tolle, K., Hoskins, E.E., Kalinichenko, V.V., Wells, S.I., Zorn, A.M., et al. (2011). Directed differentiation of human pluripotent stem cells into intestinal tissue in vitro. Nature *470*, 105–109.

Tsai, Y.-H., Czerwinski, M., Wu, A., Dame, M.K., Attili, D., Hill, E., Colacino, J.A., Nowacki, L.M., Shroyer, N.F., Higgins, P.D.R., et al. (2018). A Method for Cryogenic Preservation of Human Biopsy Specimens and Subsequent Organoid Culture. Cell. Mol. Gastroenterol. Hepatol. *6*, 218–222.e7.

Ulshen, M.H., Lyn-Cook, L.E., and Raasch, R.H. (1986). Effects of intraluminal epidermal growth factor on mucosal proliferation in the small intestine of adult rats. Gastroenterology *91*, 1134–1140.

van de Wetering, M., Sancho, E., Verweij, C., de Lau, W., Oving, I., Hurlstone, A., van der Horn, K., Batlle, E., Coudreuse, D., Haramis, A.P., et al. (2002). The β-catenin/TCF-4 complex imposes a crypt progenitor phenotype on colorectal cancer cells. Cell *111*, 241–250.

van Es, J.H., Wiebrands, K., López-Iglesias, C., van de Wetering, M., Zeinstra, L., van den Born, M., Korving, J., Sasaki, N., Peters, P.J., van Oudenaarden, A., and Clevers, H. (2019). Enteroendocrine and tuft cells support Lgr5 stem cells on Paneth cell depletion. Proc. Natl. Acad. Sci. USA *116*, 26599–26605.

VanDussen, K.L., Marinshaw, J.M., Shaikh, N., Miyoshi, H., Moon, C., Tarr, P.I., Ciorba, M.A., and Stappenbeck, T.S. (2015). Development of an enhanced human gastrointestinal epithelial culture system to facilitate patient-based assays. Gut *64*, 911–920.

Wang, Y., Gunasekara, D.B., Reed, M.I., DiSalvo, M., Bultman, S.J., Sims, C.E., Magness, S.T., and Allbritton, N.L. (2017). A microengineered collagen scaffold for generating a polarized crypt-villus architecture of human small intestinal epithelium. Biomaterials *128*, 44–55.

Wells, J.M., and Spence, J.R. (2014). How to make an intestine. Development *141*, 752–760.

Wolf, F.A., Angerer, P., and Theis, F.J. (2018). SCANPY: large-scale single-cell gene expression data analysis. Genome Biol. *19*, 15.

STAR★METHODS

KEY RESOURCES TABLE

REAGENT or RESOURCE	SOURCE	IDENTIFIER
Antibodies		
Mouse anti E-Cadherin (1:500)	BD Biosciences	Cat#610181; RRID:AB_397580
Goat anti E-Cadherin (1:100)	R&D systems	Cat#AF748; RRID:AB_355568
Rabbit anti-SM22 (1:500)	Abcam	Cat#ab14106; RRID:AB_443021
Rabbit anti-Ki67 (1:500)	Lab Vision	Cat# RM-9106-S1; RRID:AB_149792
Rabbit anti-LYSOZYME (1:800)	DAKO	Cat# A0099; RRID:AB_2341230
Mouse anti-MUC2 (1:50)	Santa Cruz Biotechnology	Cat# SC-7314; RRID:AB_627970
Donkey anti-mouse 488 (1:500)	Jackson ImmunoResearch	Cat# 715-545-150; RRID:AB_2340846
Donkey anti-rabbit 488 (1:500)	Jackson ImmunoResearch	Cat# 711-545-152; RRID:AB_2313584
Donkey anti-goat 488 (1:500)	Jackson ImmunoResearch	RRID:AB_2336933; Cat# 705-545-147
Donkey anti-mouse 647 (1:500)	Jackson ImmunoResearch	RRID:AB_2340862; Cat# 715-605-150
Donkey anti-rabbit 647 (1:500)	Jackson ImmunoResearch	Cat# 711-605-152; RRID:AB_2492288
Biological Samples		
human fetal intestine	University of Washington Laboratory of Developmental Biology	N/A
Chemicals, Peptides, and Recombinant Proteins		
EGF	R&D	236-EG
NRG1	R&D	5898-NR-050
N-acetylcysteine	Sigma	A9165-25G
Nicotinamide	Sigma	N0636-061
Critical Commercial Assays		
Neural Tissue Dissociation Kit (P)	Miltenyi	130-092-628
RNAscope® Multiplex Fluorescent Reagent Kit v2	ACD	323100
Deposited Data		
Raw scRNA-seq data (human fetal duodenum)	This study	ArrayExpress: E-MTAB-9489
Raw scRNA-seq data (human intestinal enteroids)	This study	ArrayExpress: E-MTAB-9720
Experimental Models: Cell Lines		
L-WRN Cells	ATCC	CRL-3276
Human fetal duodenal enteroids (HT-071, 142d)	This study	N/A
Human fetal duodenal enteroids (HT-323, 105d)	This study	N/A
Human fetal duodenal enteroids (HT-335 135d)	This study	N/A
Software and Algorithms		
Scanpy, Ingest	Wolf et al., 2018	https://github.com/theislab/scanpy
Cellranger	10x Genomics	https://support.10xgenomics.com/single-cell-gene-expression/software/pipelines/latest/what-is-cell-ranger
UMAP	McInnes et al., 2018	https://github.com/lmcinnes/umap
Harmony	Nowotschin et al., 2019	https://github.com/dpeerlab/Harmony
Prism 8.3.0	Graphpad	https://www.graphpad.com/scientific-software/prism/

(*Continued on next page*)

Continued

REAGENT or RESOURCE	SOURCE	IDENTIFIER
Other		
Matrigel	Corning	354234
RNAscope Probe Hs-DLL1	ACD	532631
RNAscope Probe Hs-PDGFRA-C2	ACD	604481-C2
RNAscope Probe Hs-F3-C2	ACD	407611-C2
RNAscope Probe Hs-F3	ACD	407611
RNAscope Probe Hs-WNT2B	ACD	453361
RNAscope Probe Hs-EGF	ACD	605771
RNAscope Probe Hs-EGFR	ACD	310061
RNAscope Probe Hs-ERBB2-C2	ACD	310081-C2
RNAscope Probe Hs-ERBB3	ACD	311941
RNAscope Probe Hs-NRG1-C2	ACD	311181-C2
RNAscope Probe Hs-RSPO2	ACD	423991
RNAscope Probe Hs-RSPO3-01	ACD	429851
RNAscope Probe Hs-NPY	ACD	416671
RNAscope Probe Hs-GPX3-C2	ACD	470591-C2
RNAscope Probe Hs-NRG1-C2	ACD	311181-C2
RNAscope Probe Hs-LGR5	ACD	311021
RNAscope Probe Hs-OLFM4	ACD	311041

RESOURCE AVAILABILITY

Lead Contact

Further information and requests for resources and reagents should be directed to and will be fulfilled by the Lead Contact, Jason R. Spence (spencejr@umich.edu).

Materials Availability

All unique/stable reagents generated in this study are available from the Lead Contact with a completed Materials Transfer Agreement.

Data Code and Availability

Sequencing data generated and used by this study is deposited at EMBL-EBI ArrayExpress. Datasets for human fetal intestine (ArrayExpress: E-MTAB-9489) and human fetal intestinal enteroids (ArrayExpress: E-MTAB-9720) have been deposited. Accession numbers for deposited data are also provided in the Key Resources Table. Code used to process raw data can be found at https://github.com/jason-spence-lab/Holloway_Czerwinski_Tsai_2020.

EXPERIMENTAL MODEL AND SUBJECT DETAILS

Isolating, establishing and maintaining human fetal enteroids

Fresh human fetal epithelium was isolated and maintained exactly as previously described (Tsai et al., 2018). Briefly, duodenal tissue was minced into small pieces using a scalpel under sterile conditions. To separate the epithelium from the underlying cell layers, minced biopsy specimens then were incubated in dispase (STEMCELL Technologies, 07923) for 30 minutes on ice in a Petri dish. Dispase then was removed and replaced with 100% fetal bovine serum for 15 minutes on ice. To mechanically separate the tissue layers, a volume of Advanced DMEM/F12 (GIBCO, 12634-028) equal to the initial volume of fetal bovine serum was added to the biopsy tissue before vigorously pipetting the mixture several times. Epithelial fragments then settled to the bottom of the Petri dish where they were collected manually on a stereoscope by pipet. The epithelium then was washed with ice-cold Advanced DMEM/F12 and allowed to settle to the bottom of a 1.5 mL tube. The media then was withdrawn from the loose tissue pellet and replaced with Matrigel. The Matrigel containing the isolated epithelium then was gently mixed to suspend the cells evenly before being pipetted into individual 50 μL droplets in a 24-well plate. The plate containing the droplets then was incubated at 37°C for 15 minutes to allow the Matrigel to solidify before adding media.

Once enteroids were established, Matrigel droplets were dislodged from the culture plate and were pipetted in a Petri dish. Healthy cystic enteroids were manually selected from the Petri dish under a stereoscope to be bulk-passaged through a 30G needle and embedded in Matrigel (Corning, 354234). For single-cell passaging, healthy cystic enteroids were manually selected under a stereo-

scope and dissociated with TrypLE Express (GIBCO, 12605-010) at 37°C before filtering through 40 μm cell strainers. Cells were then counted using a hemocytometer (ThermoFisher) and embedded in Matrigel. For some experiments, enteroid lines were derived in the presence of NRG1 (100 ng/ml) or NRG1 (100 ng/ml) and EGF (100 ng/ml) in addition to the standard EGF (100 ng/ml) conditions in complete LWRN media (see Media composition).

Media composition

Culture media consisted of LWRN conditioned media generated as previously described (Miyoshi and Stappenbeck, 2013; Tsai et al., 2018) and human basal media [Advanced DMEM/F12 (GIBCO, 12634-028); Glutamax 4 mM (GIBCO, 35050-061); HEPES 20 mM (GIBCO, 15630-080); N2 Supplement (2X) (GIBCO, 17502-048), B27 Supplement (2X) (17504-044), Penicillin-Streptomycin (2X) (GIBCO, 15140-122), N-acetylcysteine (2 mM) (Sigma, A9165-25G), Nicotinamide (20 mM) (Sigma, N0636-061)]. Complete media was comprised of 25% LWRN and 75% human basal media to which rhEGF (R&D, 236-EG, 100ng/ml) and/or rhNRG1 (R&D, 5898-NR-050, 100ng/ml) was added. For some experiments complete media was used without rhEGF or rhNRG1 as a control.

Human subjects

Normal, de-identified human fetal intestinal tissue was obtained from the University of Washington Laboratory of Developmental Biology. All human tissue used in this work was de-identified and was conducted with approval from the University of Michigan IRB.

METHOD DETAILS

Experimental design of enteroid cultures

The enteroid experiments in Figures 3 and 4 were carefully conducted to reduce batch effects in scRNA-seq data. All experiments comparing different treatment groups (i.e., EGF, NRG1, etc.) were carried out in parallel, with experiments and treatments being conducted at the same time. Cells were harvested and dissociated into single cell suspensions in parallel (see below). Since the 10X Chromium system allows parallel processing of multiple samples at a time, cells were captured (Gel bead-in-Emulsion - GEMS) and processed (i.e., library prep) in parallel. All samples were sequenced across the same lane(s) on a Novaseq 6000.

Single cell dissociation

To dissociate human fetal tissue to single cells, fetal duodenum was first dissected using forceps and a scalpel in a Petri dish filled with ice-cold 1X HBSS (with Mg^{2+}, Ca^{2+}). Whole thickness intestine was cut into small pieces and transferred to a 15 mL conical tube with 1% BSA in HBSS. Dissociation enzymes and reagents from the Neural Tissue Dissociation Kit (Miltenyi, 130-092-628) were used, and all incubation steps were carried out in a refrigerated centrifuge pre-chilled to 10°C unless otherwise stated. All tubes and pipette tips used to handle cell suspensions were pre-washed with 1% BSA in 1X HBSS to prevent adhesion of cells to the plastic. Tissue was treated for 15 minutes at 10°C with Mix 1 and then incubated for 10 minute increments at 10°C with Mix 2 interrupted by agitation by pipetting with a P1000 pipette until fully dissociated. Cells were filtered through a 70μm filter coated with 1% BSA in 1X HBSS, spun down at 500 g for 5 minutes at 10°C and resuspended in 500μl 1X HBSS (with Mg^{2+}, Ca^{2+}). 1 mL Red Blood Cell Lysis buffer was then added to the tube and the cell mixture was placed on a rocker for 15 minutes in the cold room (4°C). Cells were spun down (500 g for 5 minutes at 10°C) and washed twice by suspension in 2 mL of HBSS + 1% BSA, followed by centrifugation. Cells were counted using a hemocytometer, then spun down and resuspended to reach a concentration of 1000 cells/μL and kept on ice. Single cell libraries were immediately prepared on the 10x Chromium by the University of Michigan Advanced Genomics Core facility with a target of 5000 cells. The same protocol was used for single cell dissociation of healthy cystic enteroids manually collected under a stereoscope. A full, detailed protocol of tissue dissociation for single cell RNA sequencing can be found at http://www.jasonspencelab.com/protocols.

Single cell library preparation and transcriptome alignment

All single-cell RNA-seq sample libraries were prepared with the 10x Chromium Controller using either the v2 or v3 chemistry. Sequencing was performed on an Illumina HiSeq 4000 or NovaSeq 6000 with targeted depth of 100,000 reads per cell. Default alignment parameters were used to align reads to the pre-prepared hg19 human reference genome provided by the 10X Cell Ranger pipeline. Initial cell demultiplexing and gene quantification were also performed with the default 10x Cell Ranger pipeline.

Primary tissue collection, fixation and paraffin processing

Human fetal intestine tissue samples were collected as ~0.5 cm fragments and fixed for 24 hours at room temperature in 10% Neutral Buffered Formalin (NBF), and washed with UltraPure Distilled Water (Invitrogen, 10977-015) for 3 changes for a total of 2 hours. Tissue was dehydrated by an alcohol series diluted in UltraPure Distilled Water (Invitrogen, 10977-015). Tissue was incubated for 60 minutes each solution: 25% Methanol, 50% Methanol, 75% Methanol, 100% Methanol. Tissue was stored long-term in 100% Methanol at 4°C. Prior to paraffin embedding, tissue was equilibrated in 100% Ethanol for an hour, and then 70% Ethanol. Tissue was processed into paraffin blocks in an automated tissue processor (Leica ASP300) with 1 hour changes overnight.

Enteroid collection, fixation and paraffin processing

Enteroids were allowed to grow in Matrigel for several days following passaging. Once established, Enteroids in Matrigel were transferred gently with a cut pipette P1000 tip into a Petri dish filled with cold DMEM/F12. Enteroids are then manually dissected from Matrigel under a dissecting stereomicroscope using fine forceps and transferred to a microcentrifuge tube. Enteroids are left upright for several minutes until they gravity sediment to at the bottom of the tube, at which time as much media as possible is gently withdrawn. Histogel (Thermo-scientific, HG-4000-012) is slowly added to cover the enteroids following the manufacturers protocol. Once Histogel has solidified, Histogel-embedded enteroids are transferred to a 5 mL conical tube and fixed in 10% NBF overnight at room temperature. Once fixed, they are processed into paraffin as described above, sectioned and staining for FISH and IF described below.

Multiplex Fluorescent *In Situ* Hybridization (FISH) and immunofluorescence (IF)

Paraffin blocks were sectioned to generate 5 μm-thick sections within a week prior to performing *in situ* hybridization. All materials, including the microtome and blade, were sprayed with RNase-away solution prior to use. Slides were baked for 1 hour in a 60°C dry oven the night before and stored at room temperature in a slide box with a silicone desiccator packet, and with seams sealed using parafilm. The fluorescent *in situ* hybridization protocol was performed according to the manufacturer's instructions (ACD; RNAscope multiplex fluorescent manual protocol, 323100-USM) under standard antigen retrieval conditions and 30 minute protease treatment. Immediately following the HRP blocking for the C2 channel of the FISH, slides were washed three times for 5 minutes in PBS, then transferred to blocking solution (5% Normal Donkey Serum in PBS with 0.1%Tween-20) for 1 hour at room temperature. Slides were then incubated in primary antibodies overnight at 4°C in a humidity chamber. The following day, excess primary antibodies were rinsed off through a series of PBS washes. Secondary antibodies and DAPI (1 μg/ml) were added and slides were incubated at room temperature for 1 hour. Excess secondary antibodies were rinsed off through a series of PBS washes, and slides were mounted in ProLong Gold (TermoFisher, P36930). A list of antibodies and concentrations can be found in the Key Resources Table. All imaging was done using a NIKON A1 confocal and images were assembled using Photoshop CC. Z stack series were captured and compiled into maximum intensity projections using NIS-Elements (Nikon). Imaging parameters were kept consistent for all images within the same experiment and any post-imaging manipulations were performed equally on all images from a single experiment.

QUANTIFICATION AND STATISTICAL ANALYSIS

Single-cell *in silico* analysis

All *in silico* analyses downstream of gene quantification were done using Scanpy with the 10x Cell Ranger derived gene by cell matrices (Wolf et al., 2018). For primary human tissue sample analysis in Figures 1 and 2, all samples were filtered to remove cells with less than 1000 or greater than 9000 genes, less than 3500 or greater than 25000 unique molecular identifier (UMI) counts per cell. Ambient/background signal was removed from the data using CellBender. "Remove-background" was used at 200 epochs to remove ambient RNA counts from all fetal intestine samples, and the de-noised data matrix was used for subsequent analysis (Fleming et al., 2019). De-noised data matrix read counts per gene were log normalized prior to analysis. After log normalization, 2000-3000 highly variable genes were identified and extracted. The normalized expression levels then underwent linear regression to remove effects of total reads per cell and cell cycle genes, followed by a z-transformation. Dimension reduction was performed using principal component analysis (PCA) and then uniform manifold approximation and projection (UMAP) on the top 9 principal components (PCs) and 30 nearest neighbors for visualization on 2 dimensions (McInnes et al., 2018; Polański et al., 2020). Clusters of cells within the data were calculated using the Louvain algorithm within Scanpy with a resolution of 0.6. For Figures 1 and 2, combined time series data for mesenchymal and epithelial cells were integrated using Harmony to generate augmented affinity matrices and plotted as force-directed layouts with ForceAtlas2 (Jacomy et al., 2014; Nowotschin et al., 2019).

For Figures 3 and 4, all samples were filtered to remove cells with too few or too many genes (Figure 3 - < 2000, > 9000; Figures 4D–4J < 250, > 8000; Figures 4K and 4L < 500, > 3000) or with high unique molecular identifier (UMI) counts per cell (Figure 3 - 100000; Figure 4 – 10000), and a fraction of mitochondrial genes greater than 0.1-0.25. Data matrix read counts per gene were log normalized prior to analysis. After log normalization, 2000-3000 highly variable genes were identified and extracted. For Figure 3, the normalized expression levels then underwent linear regression to remove effects of total reads per cell and mitochondrial transcript fraction. Data was then scaled by z-transformation. Dimension reduction was performed using principal component analysis (PCA) and then uniform manifold approximation and projection (UMAP) on the top 11-20 principal components (PCs) and 15-30 nearest neighbors for visualization on 2 dimensions (McInnes et al., 2018; Polański et al., 2020). Clusters of cells within the data were calculated using the Louvain algorithm within Scanpy with a resolution of 0.2-0.4. Following initial PCA dimension reduction and UMAP visualization, further de-noising was not carried out for this analysis given the distinct cell clusters. In some cases, accompanying graphs were generated from summarizing the scRNA-seq data using Prism 8 software (Graphpad).

Scanpy's *Ingest* functionality was used to map enteroids onto primary human fetal epithelial cells. Epithelial cells were identified (as in Figure S1) and extracted from a data matrix to include 828 intestinal epithelial cells from ages 101, 122, 127, and 132 days (ArrayExpress: E-MTAB-9489). Epithelial cells were annotated using canonical genes (Table S3). The extracted epithelial cell matrix then again underwent log normalization, variable gene extraction, z-transformation and dimension reduction to obtain a reference embedding. *Ingest* was then run to project each of the individual enteroid datasets onto the epithelial reference map.

Cell Stem Cell, Volume *28*

Supplemental Information

Mapping Development of the Human Intestinal Niche at Single-Cell Resolution

Emily M. Holloway, Michael Czerwinski, Yu-Hwai Tsai, Joshua H. Wu, Angeline Wu, Charlie J. Childs, Katherine D. Walton, Caden W. Sweet, Qianhui Yu, Ian Glass, Barbara Treutlein, J. Gray Camp, and Jason R. Spence

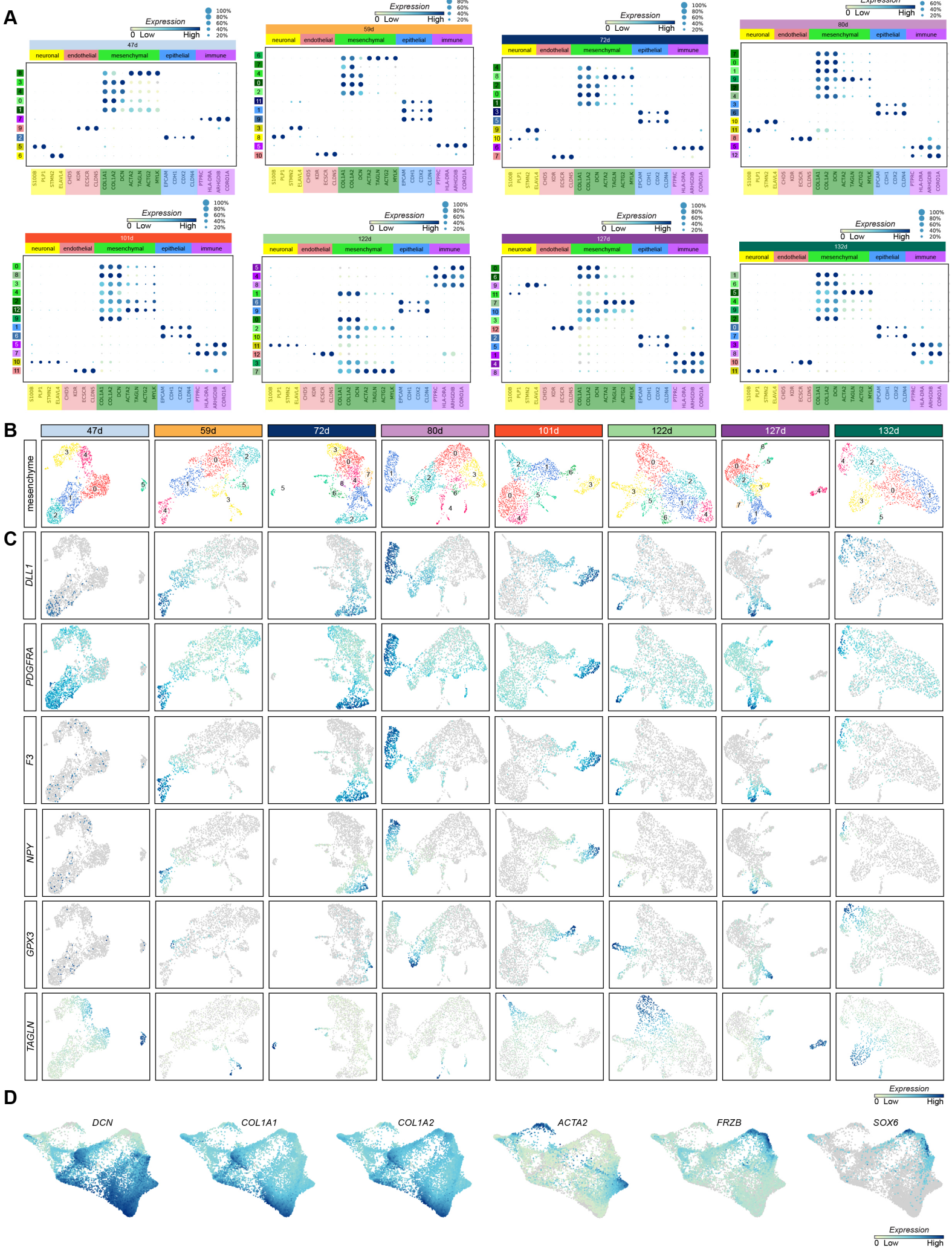
A
Expression
0 Low
High
100%
80%
60%
40%
20%
47d
59d
72d
80d
101d
122d
127d
132d
neuronal
endothelial
mesenchymal
epithelial
immune
S100B
PLP1
STMN2
ELAVL4
CHD5
KDR
ECSCR
CLDN5
COL1A1
COL1A2
DCN
ACTA2
TAGLN
ACTG2
MYLK
EPCAM
CDH1
CDX2
CLDN4
PTPRC
HLA-DRA
ARHGDIB
CORO1A
B
47d
59d
72d
80d
101d
122d
127d
132d
mesenchyme
C
DLL1
PDGFRA
F3
NPY
GPX3
TAGLN
D
Expression
0 Low
High
DCN
COL1A1
COL1A2
ACTA2
FRZB
SOX6

Supplemental Figure 1. Cell cluster annotation of primary human fetal intestine specimens profiled by scRNA-seq. Related to Figure 1. (A) Dotplot of canonical genes associated with major cell classes for each sample sequenced: Neurons (*S100B, PLP1, STMN2, ELAVL4)*; endothelium (*CDH5, KDR, ECSSR, CLDN5)*; mesenchyme (*COL1A1, COL1A2, DCN, ACTA2, TAGLN, MYLK);* epithelium (*EPCAM, CDH1, CDX2,* CLDN4); immune (*PTPRC, HLA-DRA, ARHGDIB, CORO1A*). Age is shown as days (d) post conception. (B) Mesenchymal cells from each timepoint were computationally extracted, re-clustered, and visualized using UMAP for each sample. Clusters are represented by different colors (Note: colors do not represent the same cell type for each sample). (C) Feature plots of individual genes for various mesenchymal subpopulations are shown, including *DLL1*, *PDGFRA*, *F3*, *NPY*, *GPX3*, and *TAGLN*. (D) Feature plots of additional individual genes for various lineages are shown, including *DCN*, *COL1A1*, *COL1A2*, *ACTA2*, *FRZB*, *SOX6* plotted onto the force-directed layout presented in Figure 1C.

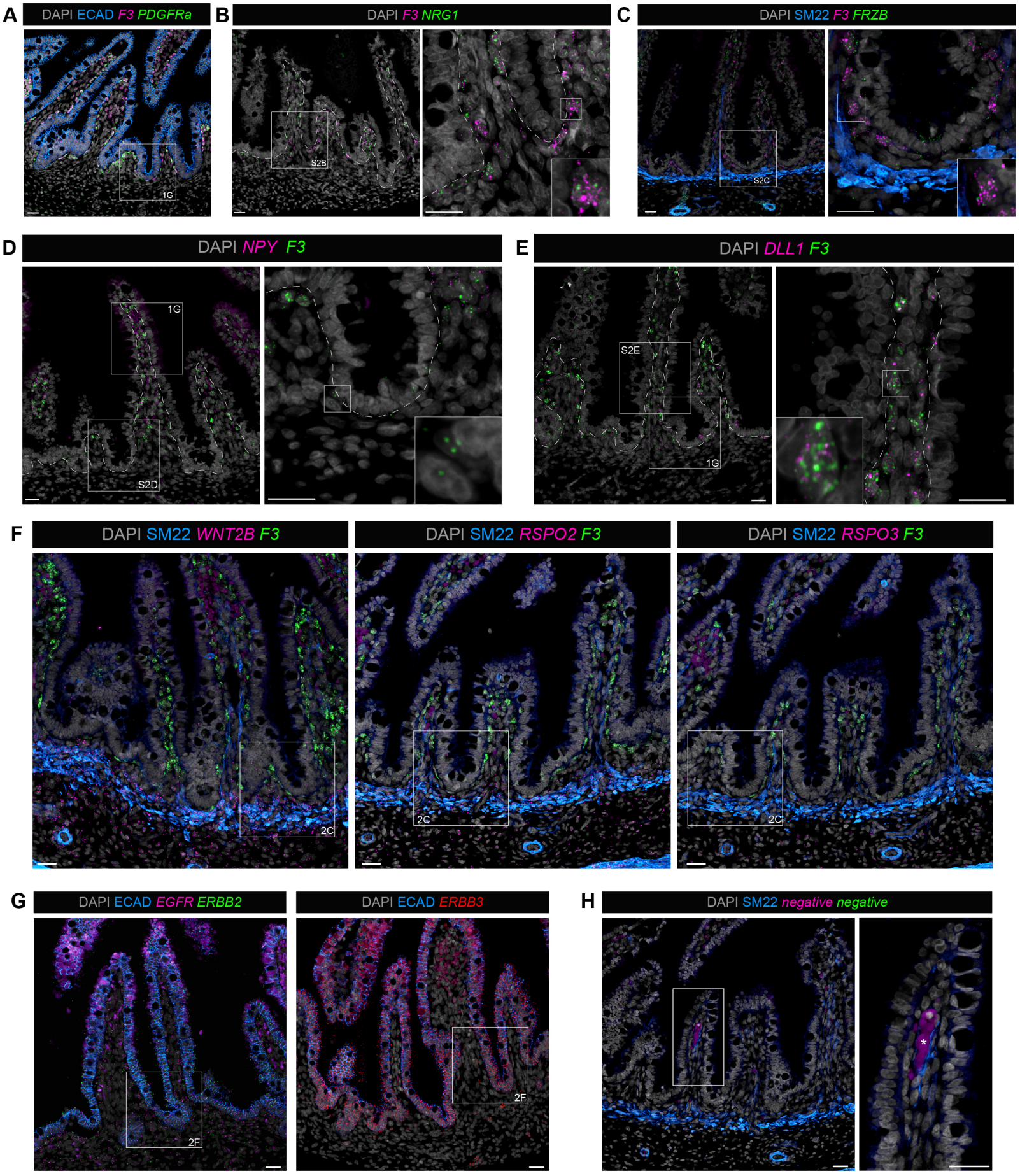
A
DAPI ECAD F3 PDGFRa
1G
B
DAPI F3 NRG1
S2B
C
DAPI SM22 F3 FRZB
S2C
D
DAPI NPY F3
1G
S2D
E
DAPI DLL1 F3
S2E
1G
F
DAPI SM22 WNT2B F3
2C
DAPI SM22 RSPO2 F3
2C
DAPI SM22 RSPO3 F3
2C
G
DAPI ECAD EGFR ERBB2
2F
DAPI ECAD ERBB3
2F
H
DAPI SM22 negative negative
*

Supplemental Figure 2. Related to Figures 1 and 2. Lower magnification imaging for spatial characterization of mesenchymal subpopulations and ISC niche factors. (A) Lower magnification image of multiplex FISH for *F3* (pink), *PDGFRa* (green) and IF for ECAD (blue) in developing human intestine (representative data shown from n = 2 biological replicates, 120d fetal sample shown). The white box indicates region that presented in Figure 1G. (B) Multiplex FISH demonstrating co-expression of *F3* (pink) and *NRG1* (green) in developing human intestine (representative data shown from n = 1 biological replicates of 132d sample). (C) Multiplex FISH demonstrating co-expression of *F3* (pink), *FRZB* (green) and IF for SM22 (blue) in developing human intestine (representative data shown from n = 2 biological replicates, 132d fetal sample shown). (D) Multiplex FISH for *NPY* (pink) and *F3* (green) in developing human intestine (representative data shown from n = 1 biological replicates of 132d sample). The upper white box indicates region that presented in Figure 1G. Note the lack of expression of *NPY* by subepithelial cells in the developing crypt region. (E) Multiplex FISH for *DLL1* (pink) and *F3* (green) in developing human intestine (representative data shown from n = 1 biological replicates of 132d sample). The lower white box indicates region that presented in Figure 1G. (F) Lower magnification image of multiplex FISH for *RSPO2, RSPO3, and WNT2B* (pink) and *F3* (green) and IF for SM22 (blue) in developing human intestine (representative data shown from n = 2 biological replicates, 120d fetal sample shown). The white boxes indicate region that presented in Figure 2C. (G) Lower magnification image of multiplex FISH for *EGFR* (pink), *ERBB2* (green), and *ERBB3* (red) and IF for ECAD (blue) in developing human intestine (representative data shown from n = 1, 132d biological replicate). White boxes indicate regions that presented in Figure 2F. (H) Representative images of multiplex FISH using commercial negative control probes (Cy3 and Cy5 channels), and IF for SM22 (blue) in developing human intestine to demonstrate tissue autofluorescence of by red blood cells and epithelium. Low level autofluorescence is consistently detected in the villus tip epithelium and blood cells (asterisk) for the 488 (pseudocolored blue) and Cy3 (pseudocolored pink) channels. Cy5 (pseudocolred green) is usually free of autofluorescence. All scalebars represent 25 μm.

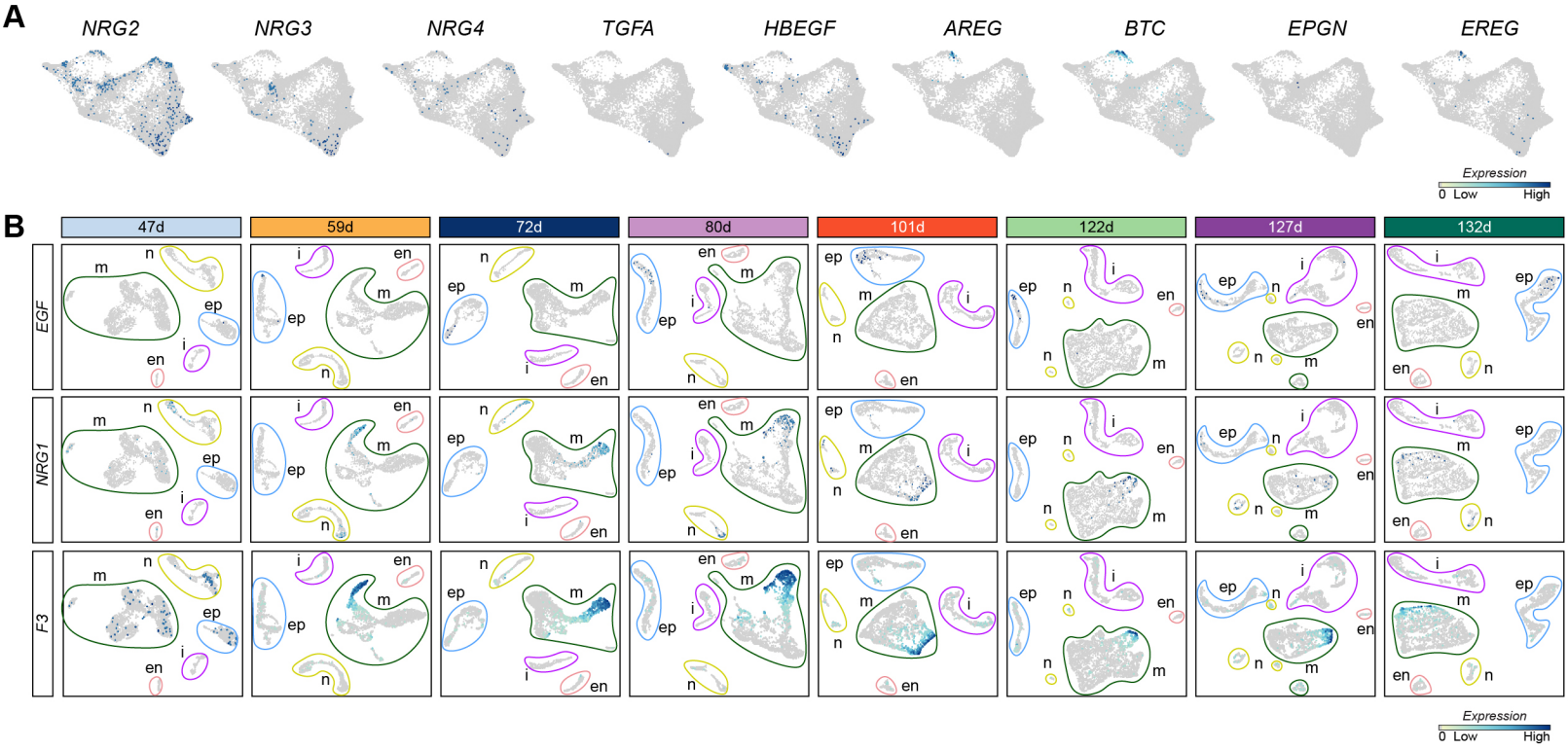
A
NRG2
NRG3
NRG4
TGFA
HBEGF
AREG
BTC
EPGN
EREG
Expression
0 Low High
B
47d
59d
72d
80d
101d
122d
127d
132d
EGF
NRG1
F3
ep
en
i
m
n
Expression
0 Low High

Supplemental Figure 3. Related to Figure 2. Investigation of EGF family ligand expression by scRNA-seq. (A) Feature plots displaying mesenchymal expression of additional EGF-family ligands *NRG2*, *NRG3, NRG4, TGFA, HBEGF, AREG, BTC, EPGN, and EREG* plotted onto the force-directed layout presented in Figure 1C. (B) Feature plots from each developmental specimen for *EGF, NRG1, and F3* interrogating expression in the entire scRNA-seq data set for each sample. Superimposed outlines demarcate epithelial (ep – blue), mesenchymal (m – green), neuronal (n - yellow), immune (i - purple), and endothelial (EC - pink) lineages.

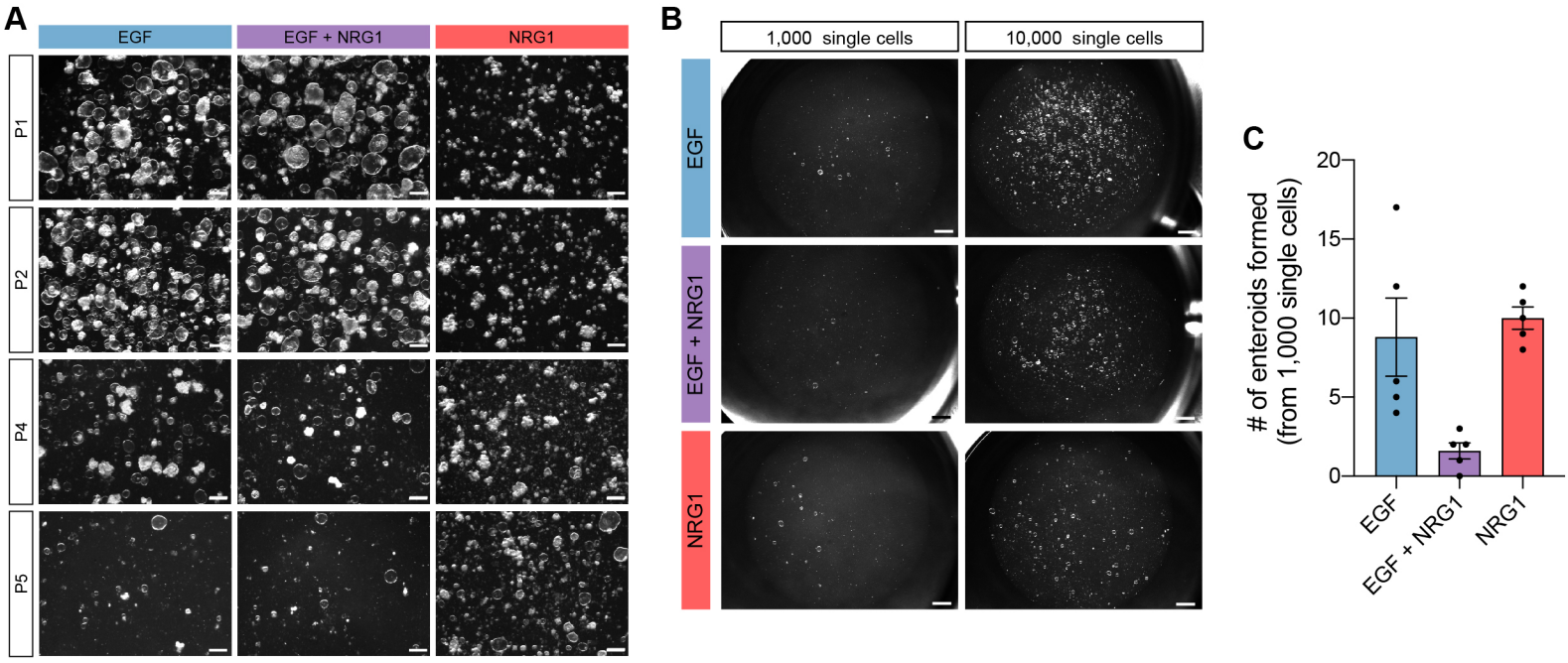
A
EGF
EGF + NRG1
NRG1
P1
P2
P4
P5
B
1,000 single cells
10,000 single cells
EGF
EGF + NRG1
NRG1
C
# of enteroids formed
(from 1,000 single cells)
20
15
10
5
0
EGF
EGF + NRG1
NRG1

Supplemental Figure 4. Enteroids established in NRG1 can be passaged at similar efficiencies to those established in standard EGF conditions. Related to Figure 4. (A) Stereomicroscope images at passage (P) P1, P2, P4, and P5 in EGF (100ng/ml), NRG1 (100ng/ml), or both EGF (100ng/ml) and NRG1 (100ng/ml). Representative data shown from n = 1, 105d biological replicate. Scalebars represent 500μm. (B) Stereoscope images of enteroids after single-cell passaging 1,000 or 10,000 cells at P2 and growth in EGF (100ng/ml), NRG1 (100ng/ml), or both EGF (100ng/ml) and NRG1 (100ng/ml). Representative data from n=1 biological replicate, 105d fetal specimen derived enteroids. Scalebars represent 1 mm. (C) Quantification of number enteroids formed from 1,000 single cells. Each data point represents 1 well of enteroids (n=5 technical replicates). Data are potted as mean ± SEM for each condition.